Zhu et al. *Zool. Res.* 2025, 46(4): 921−938
https://doi.org/10.24272/j.issn.2095-8137.2025.013
https://cstr.cn/32248.14.zr.2025.013

ZR | Zoological Research

Article Open Access

Discovery of an ancient Himalayan birch mouse lineage illuminates the evolution of the family Sicistidae (Rodentia: Dipodoidea), with descriptions of a new genus and two new species

Zhong-Xu Zhu[1,2,#], Quan Li[1,#], Wen-Yu Song[3,#], Xue-You Li[1], Andrey Lissovsky[4], Mu-Yang Wang[5], Xiao-Xin Pei[1,2], Kang Luo[1], Jing Luo[1], Ming-Jin Pu[1], Chang-Zhe Pu[1], Hong-Jiao Wang[1], Zhu Liu[6], Zhong-Zheng Chen[7,*], Xue-Long Jiang[1,*]

[1] *Key Laboratory of Genetic Evolution and Animal Models & Yunnan Key Laboratory of Biodiversity and Ecological Security of Gaoligong Mountain*, *Kunming Institute of Zoology*, *Chinese Academy of Sciences*, *Kunming*, *Yunnan* 650223, *China*

[2] *Kunming College of Life Science*, *University of Chinese Academy of Sciences*, *Beijing* 100101, *China*

[3] *Yunnan Provincial Key Laboratory for Zoonosis Control and Prevention*, *Institute of Pathogens and Vectors*, *Dali University*, *Dali*, *Yunnan* 671000, *China*

[4] *Severtsov Institute of Ecology and Evolution RAS*, *Leninskiy pr. 33*, *Moscow*119071, *Russia*

[5] *State Key Laboratory of Desert and Oasis Ecology*, *Key Laboratory of Ecological Safety and Sustainable Development in Arid Lands*, *Xinjiang Institute of Ecology and Geography*, *Chinese Academy of Sciences*, *Urumqi*, *Xinjiang* 830011, *China*

[6] *College of Life Science and Technology*, *Mudanjiang Normal University*, *Mudanjiang*, *Heilongjiang* 157011, *China*

[7] *Collaborative Innovation Center of Recovery and Reconstruction of Degraded Ecosystem in Wanjiang Basin Co-founded by Anhui Province and Ministry of Education*, *School of Ecology and Environment*, *Anhui Normal University*, *Wuhu*, *Anhui* 241002, *China*

ABSTRACT

Birch mice (family Sicistidae) are small dipodoid rodents distributed in regions surrounding the Qinghai-Xizang Plateau and extending across the Palearctic. In China, members of the genus *Sicista* are rarely recorded, and their systematics remain poorly resolved. As part of the Second Xizang Plateau Expedition by the Kunming Institute of Zoology, Chinese Academy of Sciences, systematic surveys conducted in southern Xizang and the western Tianshan Mountains yielded two previously unrecognized species. Two specimens from southern Xizang were found to occupy a deeply divergent phylogenetic position within Sicistidae. Morphological assessments and molecular phylogenetic analyses of both extant and fossil Sicistidae, along with total-evidence dating and ancestral distribution reconstruction, identified these specimens as representatives of an ancient extant lineage that diverged from *Sicista* approximately 20.38 million years ago. This lineage is designated as a new genus, defined by the new species *Breviforamen shannanensis* **gen. *et* sp. nov.** Furthermore, 11 specimens from the Tianshan Mountains are described as a second new species, *Sicista brevicauda* **sp. nov.**, based on diagnostic morphological and genetic features. Ancestral distribution reconstructions, combined with fossil records, indicate an early Miocene origin for Sicistidae across a broad region spanning the “Gobi” Desert to parts of North America. Climatic deterioration and increasing desertification during the mid-Miocene likely drove southward dispersal of *Breviforamen* **gen. nov.** into southern Xizang prior to the complete formation of the Yarlung Zangbo River. Overall, these findings broaden current understanding of Sicistidae diversity, elucidate the origin and dispersal patterns of the family, and highlight the presence of an ancient relict lineage in China.

Keywords: *Breviforamen shannanensis*; Biogeography; Phylogeny; *Sicista brevicauda*; Total evidence dating; Xizang; Xinjiang

INTRODUCTION

Birch mice (family Sicistidae) represent the most basal extant lineage within the superfamily Dipodoidea (Lebedev et al.,

Received: 21 February 2025; Accepted: 06 May 2025; Online: 07 May 2025
Foundation items: This work was supported by the Second Qinghai-Xizang Plateau Scientific Expedition and Research Program (2024QZKK0200, 2019QZKK05010100) and Survey of Wildlife Resources in Key Areas of Xizang (ZL202203601, ZL202303601)

[#]Authors contributed equally to this work

*Corresponding authors, E-mail: chenzz@ahnu.edu.cn; jiangxl@mail.kiz.ac.cn

2013), offering critical insight into the early evolutionary history of dipodoid rodents. Fossil evidence places the origin of Sicistidae in the early Miocene of Inner Mongolia, with †*Omoiosicista fui* and †*Sicista primus* representing the oldest known records (Kimura, 2010, 2011). Based on morphological features, particularly the configuration of the sinus, hyposinus, and posteroloph, Li & Qiu (2019) recognized two genera within the family: one extant (*Sicista*) and one extinct (†*Omoiosicista*). Ellerman & Morrison-Scott (1951) initially classified *Sicista* into six species—*S. betulina*, *S. caucasica*, *S. caudata*, *S. concolor*, *S. napaea*, and *S. subtilis*—according to dorsal stripe patterning, penile morphology, tail length, and hindfoot length. Subsequent revisions by Holden & Musser (2005), incorporating additional morphological characteristics, karyotypic variation, and spermatozoal traits, expanded the genus to 13 species, including seven newly identified taxa (*S. armenica*, *S. strandi*, *S.pseudonapaea*, *S. kazbegica*, *S. kluchorica*, *S. severtzovi*, and *S. tianschanica*). More recent molecular phylogenetic analyses validated *S. subtilis trizona* and *S. subtilis loriger* as distinct species and identified *S. severtzovi* as a subspecies of *S. subtilis* (Cserkész et al., 2016). Reassessment of karyotypic populations within *S. tianschanica* using genetic data led to the description of three additional species—*S. zhetysuica* (Cserkész et al., 2019), *S. terskeica* (Lebedev et al., 2021), and *S. talgarica* (Lebedev et al., 2021). Despite the presence of both fossil and extant representatives in China, comprehensive investigations remain limited and distributional data are sparse (Cheng et al., 2021).

Currently, 17 extant species of *Sicista* are recognized across Eurasia, from East Asia through Central Asia to Western Europe (Cserkész et al., 2019; Holden et al., 2017; Lebedev et al., 2021). Phylogenetic studies have resolved these extant into five major lineages and four species groups (SG): (1) the "*tianschanica*" lineage, comprising the *tianschanica* SG (*S. talgarica*, *S. terskeica*, *S. tianschanica*, and *S. zhetysuica*); (2) the "*concolor*" lineage, represented solely by *S. concolor*; (3) the "*caudata*" lineage, represented solely by *S. caudata*; (4) the "*betulina*" lineage, which includes the *subtilis* SG (*S. loriger*, *S. subtilis*, and *S. trizona*) and *betulina* SG (*S. betulina*, *S. napaea*, *S. pseudonapaea*, and *S. strandi*); and (5) the "*caucasica*" lineage, comprising the *caucasica* SG (*S. armenica*, *S. caucasica*, *S. kazbegica*, and *S. kluchorica*) (Cserkész et al., 2019; Lebedev et al., 2019).

The fossil record of Sicistidae comprises 10 formally recognized species, distributed broadly across Eurasia and North America (Green, 1977; Hall, 1930; Kimura, 2010, 2011; Qiu & Li, 2016; Qiu & Storch, 2000; Savinov, 1970; Shenbrot et al., 2008). The oldest Sicistidae representatives—†*Omoiosicista fui* and †*Sicista primus*—first appeared in Inner Mongolia during the early Miocene (Kimura, 2010, 2011), with subsequent *Sicista* fossils from both Inner Mongolia and North America dating to the middle Miocene (Green, 1977; Qiu & Li, 2016). By the late Miocene, *Sicista* showed dispersal throughout Eurasia and North America (Green, 1977; Qiu & Li, 2016; Qiu & Storch, 2000; Savinov, 1970; Tesakov et al., 2017), while Pliocene-Pleistocene records confirmed its presence in Europe, Central Asia, and Russia (Zhang et al., 2013). Despite this extensive fossil distribution, biogeographic reconstructions derived from extant species suggest that *Sicista* may have originated in the Himalaya-Tibetan Plateau and Central Asia (Pisano et al., 2015). Recent molecular divergence estimates place the split between Sicistidae and its sister families, Zapodidae and Dipodidae, at approximately 33.5 million years ago (Ma), with the extant genus *Sicista* emerging around 6.0 Ma (Lebedev et al., 2019). The ecological radiation of *Sicista* remains unresolved. Some studies have posited that lower temperatures during the Pliocene-Pleistocene transition may have driven the migration of extant *Sicista* lineages, including the "*tianschanica*," "*concolor*," and "*caucasica*" groups, as well as *S. napaea* and *S. pseudonapaea*, into mountain regions (Lebedev et al., 2019). In contrast, Cserkész et al. (2019) proposed a montane origin based on penile morphology and dorsal stripe patterning. Furthermore, efforts to reconstruct the phylogeny of Sicistidae using only extant taxa or single morphological or molecular data sources have failed to capture the complete evolutionary history (Giribet, 2015). Comprehensive phylogenetic frameworks require integrative approaches, including the total-evidence method, which unifies morphological and molecular data from both fossil and extant species, to resolve deep divergences and reconstruct ancestral relationships (Pyron, 2015).

Between 2017 and 2024, extensive field surveys were conducted across the Xizang Plateau in southwestern and western China under the Second Xizang Plateau Expedition and Research Program. These efforts yielded a substantial collection of *Sicista* specimens, including two unexpected specimens from southern Xizang —a region lacking any previous record of either extant or fossil *Sicista*. Preliminary phylogenetic analyses revealed that these specimens represent a basal lineage within Sicistidae, with a deep divergence from *Sicista*. To further investigate this discovery, a total-evidence framework integrating fossil and extant data was employed to: (1) assess species diversity and clarify the systematics of Sicistidae in China; (2) clarify the phylogenetic placement and divergence history of the newly identified lineage; and (3) propose a new hypothesis on the geographic origin and historical dispersal dynamics of Sicistidae. The findings of this study emphasize the pivotal role of the Himalayan region in driving faunal diversification and deep-time lineage persistence.

MATERIALS AND METHODS

Sample collection

Between 2017 and 2024, a total of 29 Sicistidae specimens were collected from regions surrounding the Xizang Plateau. These included two individuals from Longzi County, Shannan City in southern Xizang, 24 from the West Tianshan Mountains in Xinjiang, two from Songpan County in Sichuan, and one from Deqin County in Yunnan (Figure 1; Supplementary Table S1). In addition, 10 muscle tissue samples were obtained from Heilongjiang (China) (n=2) and Russia (n=8) (Supplementary Table S1). All animal handling procedures were conducted in accordance with the ethical standards of the Committee on Animal Protection and Ethics, Kunming Institute of Zoology, Chinese Academy of Sciences (approval no. SMKX-20191020-212). During fieldwork, external measurements were recorded, skins were prepared, and muscle tissues were preserved in anhydrous ethanol and stored at −80°C. Skulls were later cleaned in the laboratory. All newly generated sequences were deposited in GenBank under accession numbers PV175483–PV175516, PV263066–PV263139, PV298461–PV298532, PV335386, PV335313–PV335385, PV339659–PV339670, and PV339674–PV339710

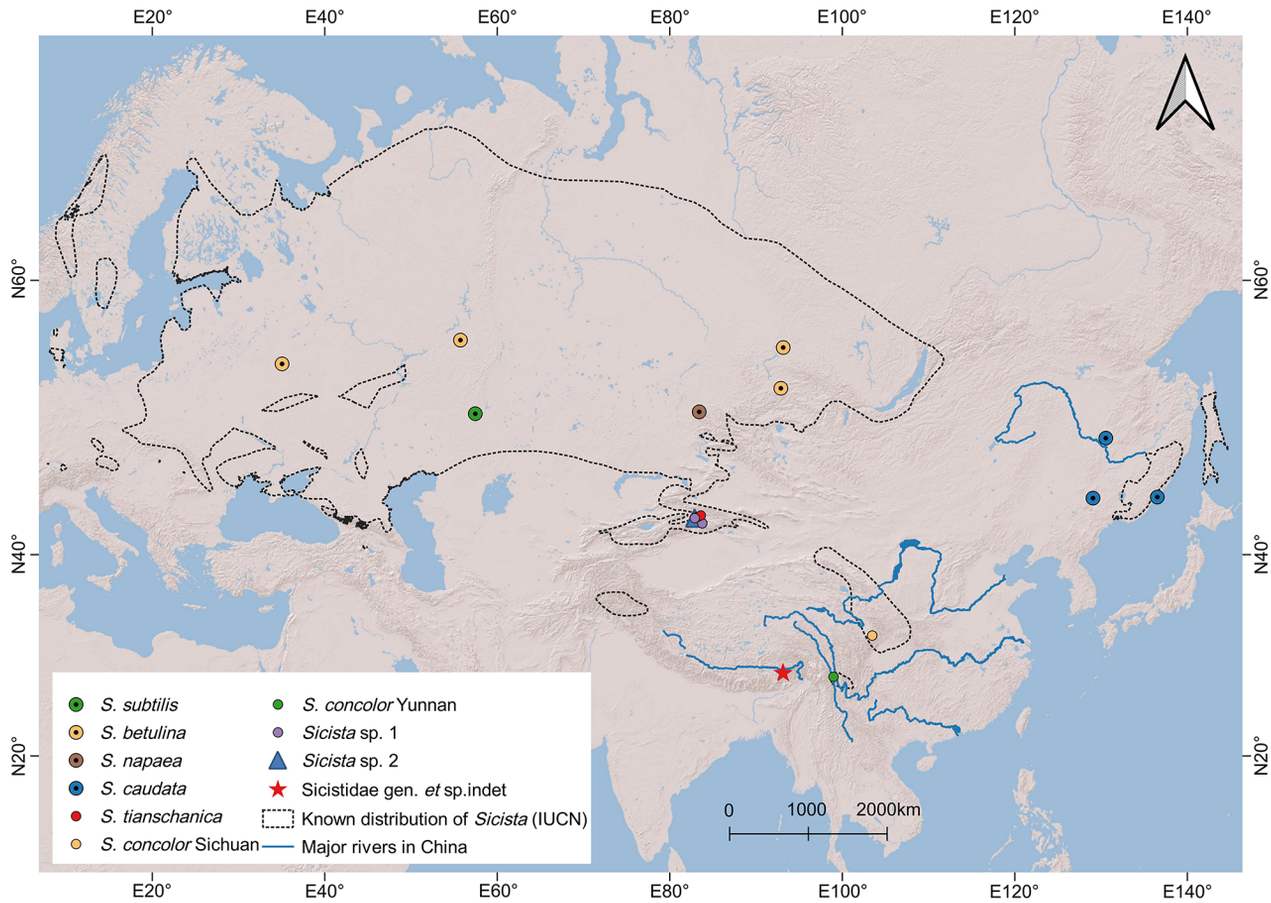

Figure 1 Sampling localities of specimens used in the study

Specific specimen sampling areas are shown in Supplementary Table S1.

(Supplementary Table S1) and uploaded to ScienceDB (www.scidb.cn/doi/10.24272/j.issn.2095-8137.2025.013).

Preliminary species identification was performed using a phylogenetic framework based on mitochondrial cytochrome b (cyt *b*; 1 140 bp), incorporating reference sequences from GenBank (Supplementary Table S2). Combining phylogenetic clustering with geographic sampling location, six known operative taxonomic units (OTUs) and three undescribed OTUs were identified (Supplementary Table S1). The known OTUs included: *S. concolor* (*n*=3) from Yunnan and Sichuan; *S. tianschanica* (*n*=3) from Xinjiang; *S. caudata* (*n*=4) from Heilongjiang (China) and the Primorskiy Territory and Amur Region (Russia); *S. subtilis* (*n*=1) from the Orenburg region (Russia); *S. betulina* (*n*=4) from the Krasnoyarskiy Territory, Bashkiria Republic, and Smolensk Region (Russia); and *S. napaea* (*n*=1) from the Altaiskiy Territory (Russia).

The two specimens from southern Xizang exhibited distinctly shortened incisive foramina, a feature not observed in the genus *Sicista* (Cserkész et al., 2019; Holden et al., 2017; Lebedev et al., 2021), and were recovered as a sister lineage to *Sicista* based on the cyt *b* phylogeny (Figure 2). These individuals were consequently designated as a putative new genus within Sicistidae —Sicistidae gen. *et* sp. indet. —based on distinct morphological characteristics and their phylogenetic position within the broader cyt *b* framework. In the West Tianshan Mountains in Xinjiang, 11 specimens possessed significantly shorter tails than any known non-striped *Sicista* species and were therefore designated as a putative new species (*Sicista* sp. 1). An additional 10 specimens from the same region, although morphologically similar to *S. tianschanica*, formed a distinct monophyletic clade in the cyt *b* phylogeny and were thus assigned to a second putative new species (*Sicista* sp. 2).

Morphological data and analysis

Two morphological data types were compiled for both fossil and extant species: (1) morphometric measurements, primarily for comparative analysis of extant species, and (2) a morphological coding matrix incorporating both fossil and extant taxa. Two juvenile *Sicista* sp. 1 specimens, identified by the eruption of the third upper molar, were excluded from all morphometric analyses. Morphological measurements and character assessments were performed on the remaining 27 specimens. Five external measurements (body weight, head-body length, tail length, hindfoot length, and ear length) were recorded from specimen labels. Intergroup variation in external morphology was visualized using range and scatter plots of traits that showed significant differences based on Kruskal-Wallis tests, implemented with the ggplot2 package (v3.3.3; Wickham, 2016). Cranial measurements followed Kimura (2011) and Lebedev et al. (2021), covering 28 skull and dental metrics (P for premolars, M for molars, superscript for upper premolars and upper molars, subscript for lower premolars and lower molars): greatest length of skull (GLS), condylo-incisive length (CIL), zygomatic width (ZW), incisive foramen length (IFL), palatine bridge length (PBL), greatest palatal breadth (GPB), zygomatic width at infraorbital foramina (ZFW), foramen magnum width (FMW), mesopterygoid fossa width (MEPFW), incisive width (IW), nasal width (NASW),

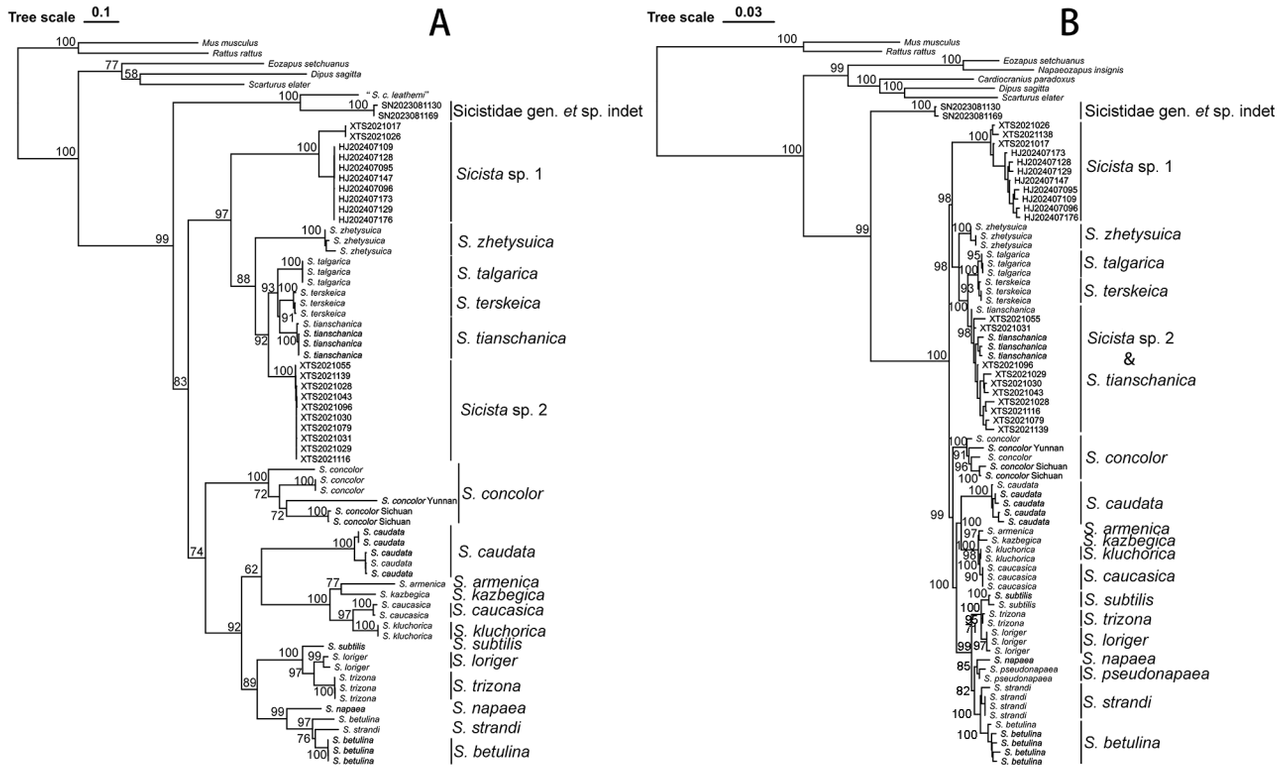

Figure 2 Results of maximum-likelihood phylogenetic analyses

A: Mitochondrial gene tree. B: Concatenated nuclear gene tree. Tip labels in bold indicate new specimens in this study.

interorbital width (IOW), auditory bulla width (BULW), maxillary toothrow length (P^4–M^3), maxillary molar row length (M^1–M^3), M^1 length (M^1L), M^3 length (M^3L), M^2 width (M^2W), M^3 width (M^3W), mandibular molar row length (M_1–M_3), M_2 length (M_2L), M_3 length (M_3L), M_1 width (M_1W), M_2 width (M_2W), M^2 length (M^2L), M^1 width (M^1W), M_1 length (M_1L), and M_3 width (M_3W) (Supplementary Figure S1). Due to the small size of *Sicista* skulls, larger structures (e.g., greatest length of skull, maxillary toothrow length) were measured with electronic vernier calipers (0.01 mm), while smaller structures (e.g., M^1 length, M^1 width) were measured using a Keyence 2000 microscope camera at 200× magnification. Incisive foramen morphology was examined across 17 *Sicista* species using a combination of textual descriptions, photographs, and physical specimens. This assessment included materials from both online collections —such as the United States National Museum of Natural History and Siberian Zoological Museum of the Institute of Animal Systematics and Ecology, Siberian Branch of the Russian Academy of Sciences (Novosibirsk, Russia) —and in-person reviews conducted at the Kunming Natural History Museum of Zoology, Kunming Institute of Zoology, Chinese Academy of Sciences, and National Animal Collection Resource Center (NACRC), China (Supplementary Table S3).

Phylogenetic analyses

Morphological tree: Morphological characteristics of external features, skulls, and molars were documented, with molar images captured using a Keyence 2000 microscope camera. Trait coding followed Kimura (2011) and Daxner-Höck et al. (2014) (Supplementary Table S4). These newly coded traits were integrated with an existing morphological matrix of 14 fossil genera compiled from previous studies (Calede et al., 2022; Kimura, 2013). Phylogenetic reconstruction based on this combined dataset was performed using the maximum parsimony method in PAUP* (Swofford, 2002), generating both strict consensus and 50% majority-rule trees. This approach aimed to determine whether the new specimens correspond to any known fossil taxa and to resolve their relationships within Sicistidae. A heuristic search was conducted under the parsimony criterion, with 1 000 replicates of stepwise random and tree bisection-reconnection (TBR) branch swapping. Multiple trees were saved. Morphological characters 5, 6, 31, and 38 were ordered (Calede et al., 2022).

Molecular tree: Genomic DNA was extracted using the Qiagen DNeasy Blood and Tissue Kit. As phylogenetic analyses of *Sicista* require a sufficiently large number of gene fragments for adequate resolution (Lebedev et al., 2019), one mitochondrial gene fragment (cyt *b*) and eight nuclear gene fragments — *BRCA1* (exon 11 of the breast cancer type 1 susceptibility protein gene; 816 bp), *BRCA2* (exon 11 of the breast cancer type 2 susceptibility protein gene; 963 bp), *GHR* (exon 10 of the growth hormone receptor; 915 bp), *IRBP* (exon 1 of the interphotoreceptor binding protein gene; 1 197 bp), *RAG1* (recombination activating protein gene 1; 1 056 bp), *RAG2* (recombination activating protein gene 2; 885 bp), *STPBN* (intron 13 of the beta-spectrin 1 gene; 692 bp), and *THY* (intron 2 of the thyrotropin gene; 675 bp)—were amplified and sequenced from 39 specimens. Primer sequences are listed in Supplementary Table S5. All polymerase chain reaction (PCR) products were sequenced bidirectionally on an ABI 3730 Genetic Analyzer (Applied Biosystems, USA).

To include all 17 extant *Sicista* species in the phylogenetic analysis, mitochondrial and nuclear gene fragments for 16 species were downloaded from GenBank (Supplementary Table S2). The final dataset, incorporating newly sequenced and public data, encompassed the full extant diversity of *Sicista*. Outgroup taxa included *Scarturus elater* Lichtenstein,

1825, *Cardiocranius paradoxus* Satunin, 1903, *Eozapus setchuanus* Pousargues, 1896, *Napaeozapus insignis* Miller, 1891, *Dipus sagitta* Pallas, 1773, *Mus musculus* Linnaeus, 1758, and *Rattus rattus* Linnaeus, 1758.

Two molecular datasets were constructed: (1) a mitochondrial cyt *b* dataset with 15.6% missing data and (2) a concatenated nuclear dataset with 38.7% missing data. Partition schemes and evolutionary models were determined using PartitionFinder 2 (Lanfear et al., 2012) within the PhyloSuite v.1.2.3 platform (Zhang et al., 2020). The best models for each dataset are listed in Supplementary Table S6. Phylogenetic trees were constructed using maximum-likelihood (ML) and Bayesian inference (BI) analyses implemented in IQ-TREE 2 v.2.3.6 (Minh et al., 2020) and MrBayes v.3.2.7a (Ronquist et al., 2012), respectively, both within PhyloSuite v.1.2.3. ML analysis included 5 000 ultrafast bootstrap replicates, whereas BI analysis was run for 2 000 000 generations with sampling every 1 000 generations and a burn-in set to 0.25. Node support was considered strong under ultrafast bootstrap (UFBoot) values ≥95 and posterior probability (PP) values ≥0.95 (Huelsenbeck & Rannala, 2004; Minh et al., 2018).

Divergence time estimation

Node dating and total-evidence tip dating represent two widely applied approaches for estimating divergence times. Node dating is typically limited to extant taxa, while total-evidence tip dating can sometimes conflict with fossil evidence (Luo et al., 2021; O'Reilly & Donoghue, 2016). To overcome these limitations, total-evidence tip-and-node dating was employed, integrating their respective strengths to improve temporal inference accuracy (O'Reilly & Donoghue, 2016). Moreover, the inclusion of fossil data has been shown to enhance the reliability of ancestral distribution reconstructions (Faurby et al., 2024). The total-evidence tip-and-node dating analyses incorporated both morphological and nuclear sequence matrices. In the morphological phylogeny, several fossil taxa exhibited uncertain placements in both the strict consensus and 50% majority-rule topologies. In contrast, the nuclear gene tree provided well-resolved relationships among extant species. To reduce the impact of topological ambiguity on divergence time estimation (dos Reis et al., 2015), seven fossil taxa, including †*S. wangi*, †*Sicista* sp. from Bartlett, †*S. ertemteensis*, †*S. bagajevi*, †*S. bilikeensis*, †*S. praeloriger*, and *S. c. leathemi*, were excluded from the analysis due to unresolved positions in both datasets. Priors were specified only for taxa with well-supported phylogenetic relationships.

Divergence time estimation was conducted in BEAST v.2.7.7 (Bouckaert et al., 2014) using the morphological matrix and nuclear gene dataset. The cyt *b* gene was excluded due to potential underestimation of estimates for ancient taxa (Lebedev et al., 2019). Two fossil and two secondary calibrations were applied, and all priors were implemented under the "mean in real space" parameter:

● Earliest myodont, *Erlianomys* (55.8–48.6 Ma) (Li & Meng, 2010): Log-normal prior with M=52.0 and S=0.04.

● Earliest split between *Mus* and *Rattus*: *Antemus* (~14.0 Ma), *Progonomys* (10.4–12.3 Ma), and *Karnimata* (~11.1 Ma) (Jaeger et al., 1986): After correction by Kimura et al. (2015) and following Camacho-Sanchez & Leonard (2020), the time of separation between *Mus* and *Rattus* was estimated at 11.11–12.68 Ma. Log-normal prior with M=11.81 and S=0.035.

● Time of separation between *subtilis* SG and *betulina* SG (2.2–3.1 Ma) (Lebedev et al., 2019), aligning with fossil evidence: Log-normal prior with M=2.6 and S=0.1.

● Time of separation between Cardiocraniinae and other dipodids (18.1–23.1 Ma) (Shenbrot et al., 2017): Log-normal prior with M=20.4 and S=0.07.

The best substitution models were determined using PartitionFinder 2 (Lanfear et al., 2012). Molecular clock models were assessed via path sampling and stepping-stone sampling in BEAST v.1.10.4 (Baele et al., 2012; Suchard et al., 2018), as this feature can only be implemented in BEAST v.1. Relaxed molecular clocks were favored for all genes except for *RAG2*, which followed a strict molecular clock. Morphological data were analyzed under the MK model (Lewis, 2001), and the fossilized birth-death (FBD) model (Stadler, 2010) was applied as the prior setting. Two independent analyses were run for 400 000 000 generations, with sampling every 1 000 iterations. Parameter settings followed those described by Luo et al. (2021). Convergence diagnostics were performed in Tracer v.1.7 (Rambaut et al., 2018), with effective sample size (ESS) values ≥200 indicative of convergence. Phylogenetic trees were visualized ("landscaped") using tvBOT (Xie et al., 2023).

Ancestral area reconstruction

Ancestral distribution reconstruction was performed using BioGeoBEARS (Massana et al., 2015; Matzke, 2013, 2014a, 2014b) implemented in RASP v.4.3 (Yu et al., 2020). Geographic regions were delineated based on the biogeographic frameworks proposed by Pisano et al. (2015) and Lebedev et al. (2019), together with species range data obtained from IUCN (2024). The distribution of Sicistidae was as follows: A: West Palearctic, B: North America, C: Siberia, Far East and South-East Russia, D: Kazakh Steppe, E: Xizang Plateau and surrounding mountains, and F: "Gobi" (current Gobi Desert region) and surrounding areas. As Sicistidae distributions do not encompass more than three areas, each node was restricted to a maximum of three areas. Six models of range evolution were tested (DEC, DEC+J, DIVALIKE, DIVALIKE+J, BAYAREALIKE, and BAYAREALIKE+J) using BioGeoBEARS in RASP v.4.3. The BAYAREALIKE model emerged as the most suitable based on AICc_wt ranking (Supplementary Table S7).

RESULTS

Morphological variation

External and cranial measurements of 27 Sicistidae specimens are summarized in Supplementary Table S8, with comparative box plots shown in Figure 3. Among these, Sicistidae gen. *et* sp. indet. and *S. tianschanica* exhibited the largest body sizes within the family (head-body length (HB): Sicistidae gen. *et* sp. indet. mean=78.5 mm, range=77–80 mm; *S. tianschanica* mean=78.3 mm, range=75–80 mm). *Sicista concolor* was smaller than Sicistidae gen. *et* sp. indet. and *S. tianschanica* but larger than the other *Sicista* species (HB: *S. concolor* mean=71.3 mm, range=68–76 mm; *Sicista* sp. 1 mean=65 mm, range=60–70 mm; *Sicista* sp. 2 mean=70.5 mm, range=65–80 mm). Tail length differed markedly across species, with *Sicista* sp. 1 showing the shortest tail among species from the Tianshan region (*Sicista* sp. 1 TL=73.4±2.62 mm, TL/HB ratio=113%; *S. tianschanica* TL=116.3±6.66 mm, TL/HB ratio=149%; *Sicista* sp. 2

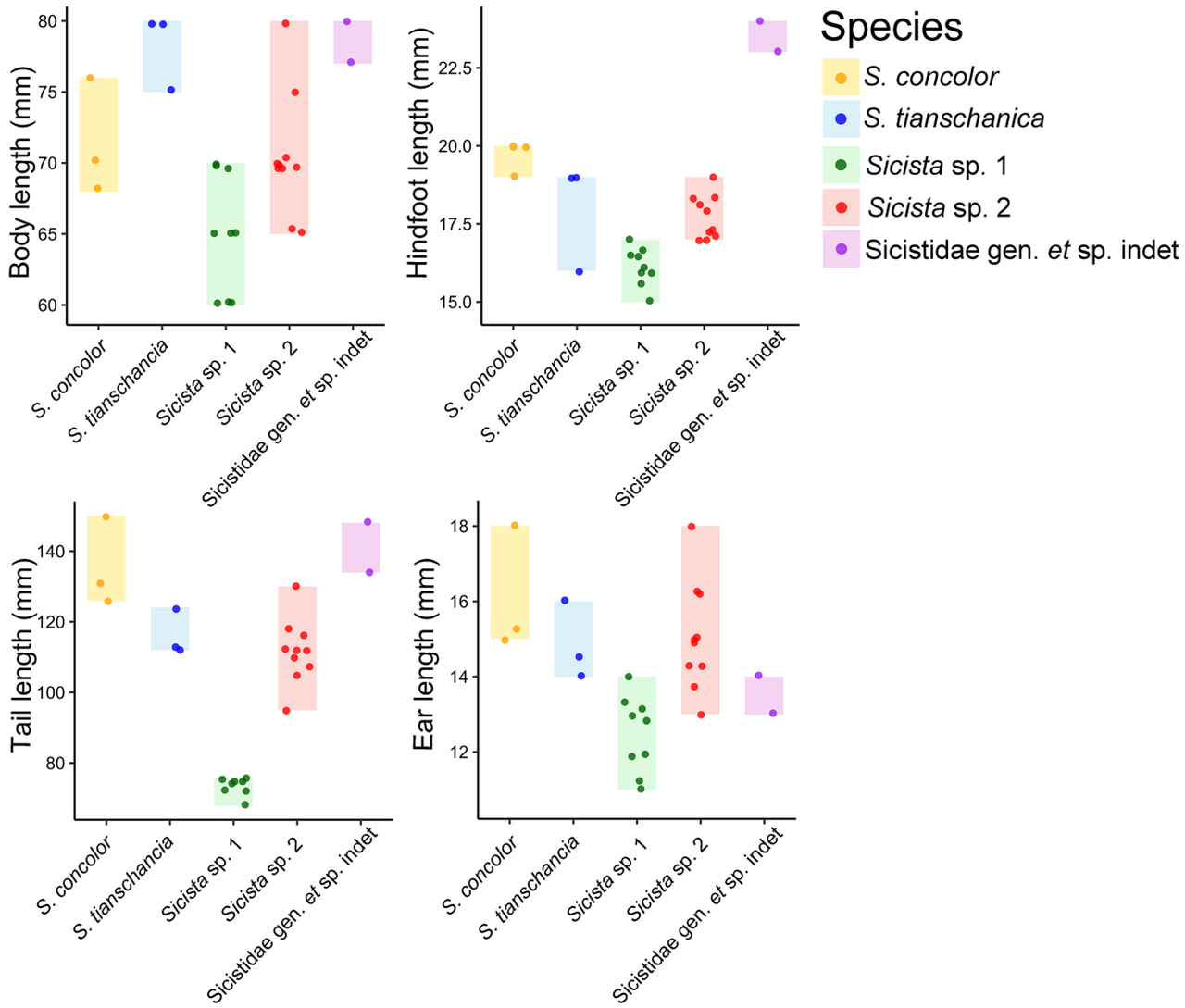

Figure 3 Range and scatter plots showing significant differences in four external measurements among five taxa, based on Kruskal-Wallis tests.

TL=111.7±9.08 mm, TL/HB ratio=158%). Morphologically, *Sicista* sp. 1 was distinguished by the absence of a dorsal stripe, in contrast to the presence of a striped dorsum in *S. subtilis*, *S. betulina*, *S. strandi*, *S. trizona*, and *S. loriger*. It also differed from unstriped taxa such as *S. napaea* and *S. pseudonapaea* by its significantly shorter tail length. *Sicista* sp. 2 showed a larger body size than *S. zhetysuica*, *S. terskeica*, and *S. talgarica* but was smaller than *S. tianschanica* (HB: *Sicista* sp. 2 mean=70.5±4.38 mm; *S. tianschanica* mean=78.3±2.89 mm). Its tail length exceeded that of most species in the genus but was shorter than that of *S. tianschanica* in the Tianshan Mountains. Sicistidae gen. *et* sp. indet. possessed the longest hind foot among the examined specimens (23–24 mm vs. 13–22 mm), surpassing the maximum recorded length for the genus *Sicista*. Hind foot length varied across species: *S. concolor*, *S. tianschanica*, and *Sicista* sp. 2 exhibited relatively long hind feet, whereas *Sicista* sp. 1 showed short hind feet, comparable to those of *S. terskeica*, *S. zhetysuica*, and *S. caudata*. All comparative data are presented in Supplementary Tables S8 and S9.

Phylogenetic relationships

Morphological tree: Both the strict consensus and majority-rule trees derived from 256 maximum parsimony trees (tree length: 347; CI=0.559; RI=0.740; RC=0.414; HI=0.793) resolved Sicistidae into three subclades: Sicistidae gen. *et* sp. indet., † *Omoiosicista fui*, and *Sicista*. † *Omoiosicista* was recovered as the most basal lineage within the family, followed by Sicistidae gen. *et* sp. indet., with *Sicista* forming the crown group (Figure 4). Within the *Sicista* clade, † *S. gemmacollis* was placed as the basal sister group to all other species, with † *S. primus* identified as the second-most basal lineage. Phylogenetic relationships among the remaining *Sicista* species remain unresolved, with both tree topologies displaying comb-like or polytomous branching patterns.

Molecular tree: Both the ML and BI analyses based on molecular data yielded similar topologies (Figure 2; Supplementary Figure S2). All reconstructions strongly supported Sicistidae gen. *et* sp. indet. as a monophyletic group (PP=1.00, UFBoot=100), which was recovered as the sister group to the genus *Sicista* (PP=1.00, UFBoot=99). Within *Sicista*, five major clades were resolved, consistent with those outlined in the introduction. The "*tianschanica*" lineage occupied the basal position within the genus. Within the "*tianschanica*" lineage, *Sicista* sp. 1 formed a monophyletic group (PP=1.00, UFBoot=100) and was placed at the base of the lineage (PP=1.00, UFBoot=97–98). *Sicista* sp. 2 also

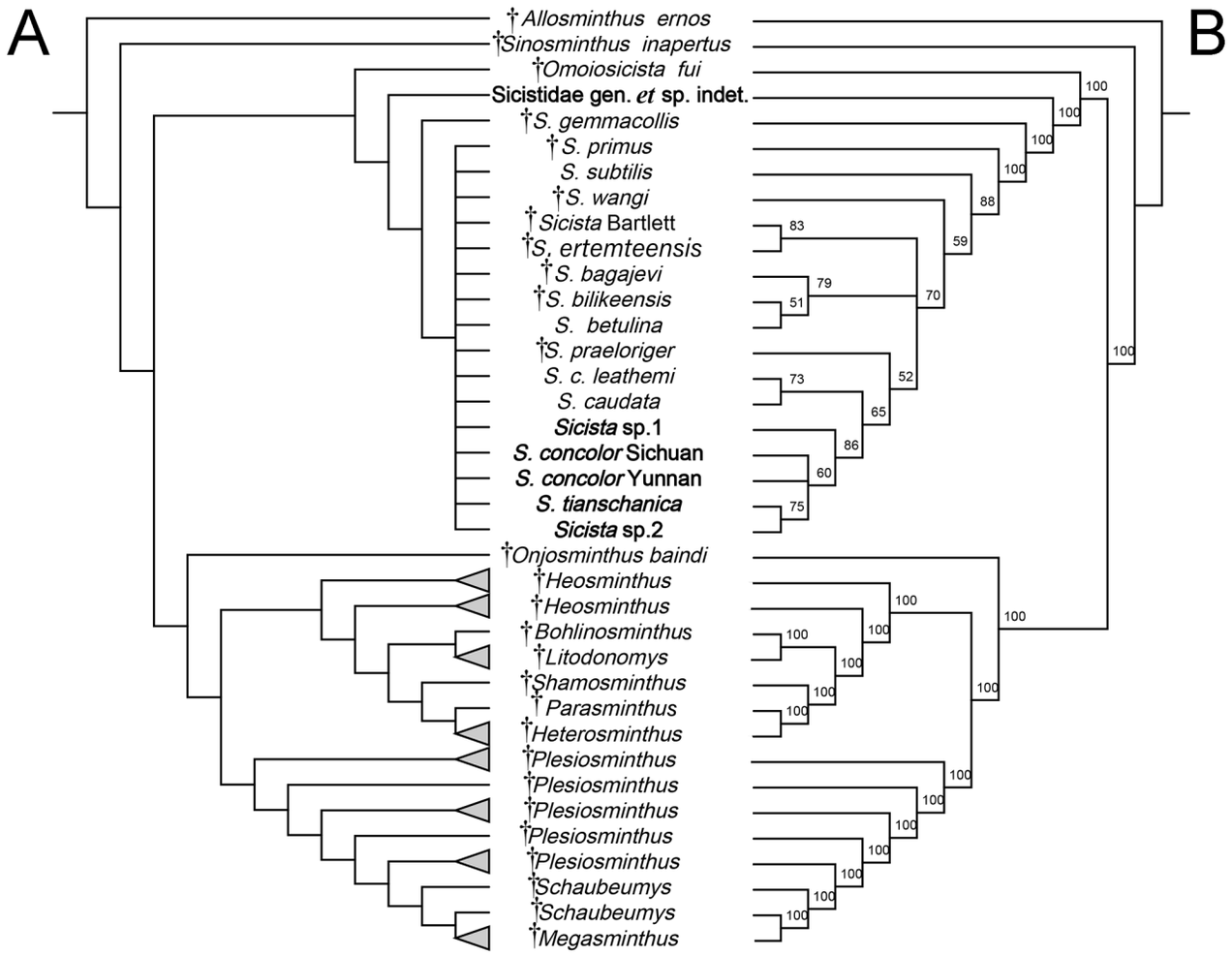

Figure 4 Phylogenetic tree of Sicistidae obtained from maximum-parsimony analysis based on morphological matrix

A: Strict consensus tree from the 256 most parsimonious trees. B: 50% majority-rule tree from the 256 most parsimonious trees. Node values in B indicate the percentage of trees supporting each relationship. Tip labels in bold indicate new specimens in this study.

formed a well-supported monophyletic clade (PP=1.00, UFBoot=100) in the mitochondrial gene tree, where it appeared as sister to *S. talgarica*, *S. terskeica*, and *S. tianschanica* (PP=1.00, UFBoot=92). However, in the nuclear gene tree, *Sicista* sp. 2 and *S. tianschanica* formed a monophyletic group with strong support (PP=1.00, UFBoot=98). The "*concolor*" lineage represented the second-most basal group within *Sicista*, with specimens from Qinghai positioned at the base of the clade (PP=1.00, UFBoot=100). The "*caudata*" and "*caucasica*" lineages together formed a sister group to the "*betulina*" lineage (PP=0.90–1.00, UFBoot=92–100), with the "*caudata*" lineage positioned as sister to the "*caucasica*" lineage (PP=0.70–1.00, UFBoot=62–100).

Divergence times

The total-evidence tip-and-node dating results (Figure 5) revealed that the divergence between †*Omoiosicista* and the Sicistidae gen. *et* sp. indet. + *Sicista* lineage occurred ca. 24.71 million years ago (Ma) (95% confidence interval (CI): 18.84–31.77 Ma). Sicistidae gen. *et* sp. indet. diverged from *Sicista* around 20.38 Ma (95% CI: 17.40–24.02 Ma). Within the *Sicista* clade, † *S. gemmacollis* separated from other *Sicista* species ca.18.47 Ma (95% CI: 17.00–21.63 Ma), while † *S. primus* diverged from recent *Sicista* species ca. 17 Ma (95% CI: 17.00–18.79 Ma). The estimated divergence times for the five major lineages within the genus *Sicista* are as follows:

● The "*tianschanica*" lineage diverged from other *Sicista* species around 6.78 Ma (95% CI: 5.59–8.15 Ma), with *Sicista* sp. 1 splitting from other "*tianschanica*" species approximately 6.04 Ma (95% CI: 4.75–7.50 Ma).

● The "*concolor*" lineage separated from the "*caudata*" + "*caucasica*" + "*betulina*" lineage around 6.04 Ma (95% CI: 4.96–7.26 Ma).

● The "*betulina*" lineage diverged from the "*caudata*" + "*caucasica*" lineage approximately 5.26 Ma (95% CI: 4.32–6.36 Ma).

● The "*caudata*" lineage split from the "*caucasica*" lineage around 4.75 Ma (95% CI: 3.77–5.82 Ma).

Ancestral distribution reconstruction

The family Sicistidae likely originated from the "Gobi" region combined with North America during the Late Oligocene to Early Miocene, with a probability of 15.96%. This was followed by the "Gobi" region alone (13.14%) and the combined regions of "Gobi," North America, and the Xizang Plateau (11.37%). The most probable ancestral region for Sicistidae gen. *et* sp. indet. was the "Gobi" region (probability=24.80%) or the "Gobi" region combined with North America (probability=27.97%). For

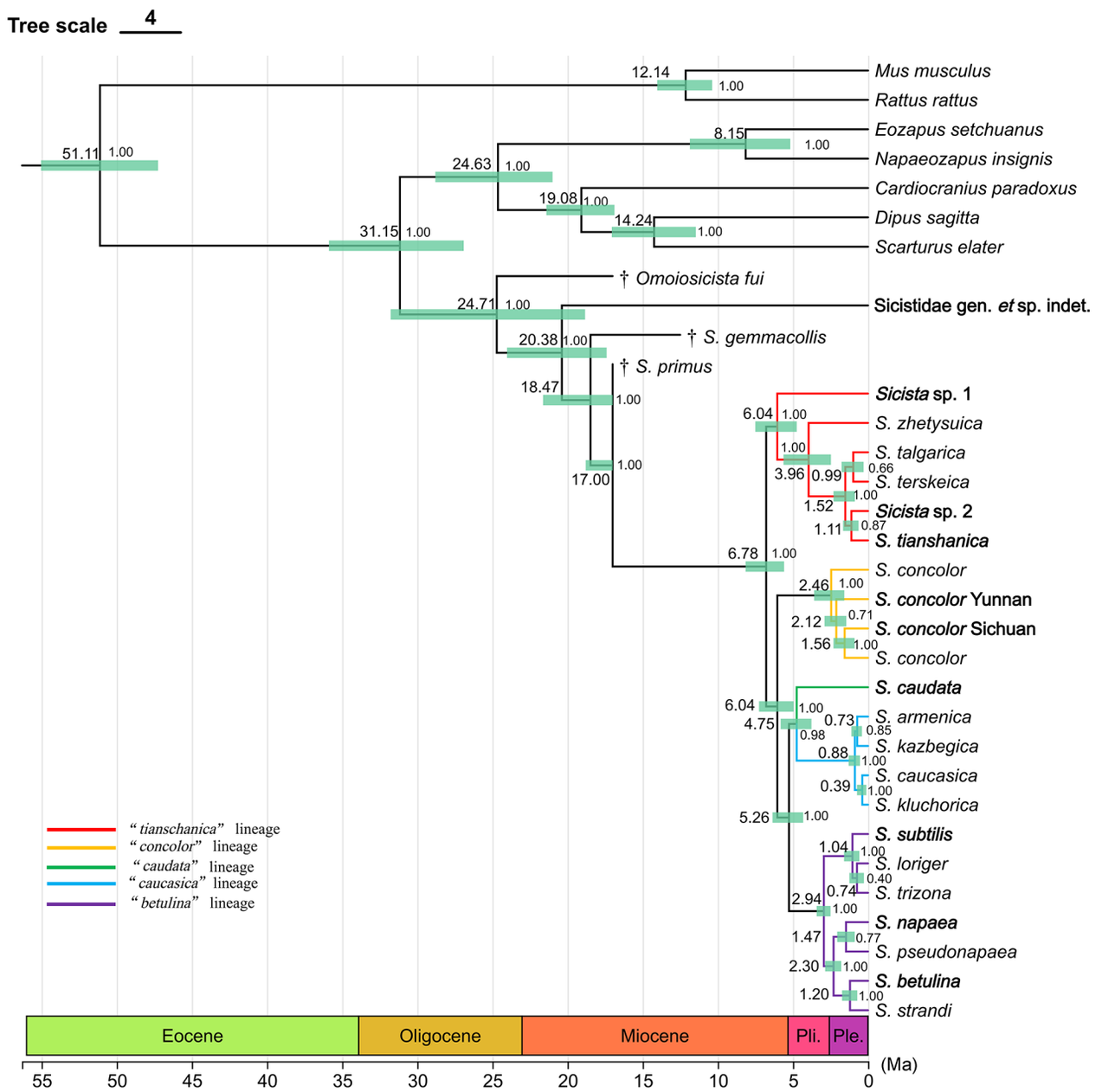

Figure 5 Divergence times estimated using BEAST based on concatenated nuclear dataset and morphological matrix

Large node values indicate divergence times (Ma) and smaller node values indicate Bayesian posterior probabilities. Tip labels in bold indicate new specimens from this study.

the genus *Sicista*, the ancestral distribution was most likely in the combined regions of "Gobi" and North America (41.40%) or the "Gobi" region alone (40.21%). Excluding † *S. gemmacollis*, which originated in the Americas, the remaining *Sicista* species were most likely derived exclusively from the "Gobi" region, with a probability of 100%. Additionally, the extant *Sicista* species are most likely to have originated from the Xizang Plateau and its surrounding mountains, with a probability of 39.47% (Figure 6).

DISCUSSION

Taxonomic evaluation of the new lineages

Integrative analyses combining morphological and molecular datasets supported the monophyly of Sicistidae gen. *et* sp. indet., recovered as the sister lineage to *Sicista* within Sicistidae (Figures 2, 4). Divergence dating placed the origin of this lineage in the early Miocene, approximately 20.38 Ma, predating all extant *Sicista* species. A key morphological trait distinguishing Sicistidae gen. *et* sp. indet. was the incisive foramen, which did not extend to the anterior edge of the premolars—a condition absent in any known *Sicista* species. In contrast, all examined *Sicista* specimens, including those from Kashmir in the western Himalayas, showed incisive foramen that extended beyond a line drawn from the anterior edge of P^4 (Supplementary Table S3). Zagorodniuk (2021) posited that incisive foramina are generally taxon-specific at both the genus and family levels, often reflecting distinct morphological patterns across rodents, with *Sicista* serving as a representative example of genus-level specificity.

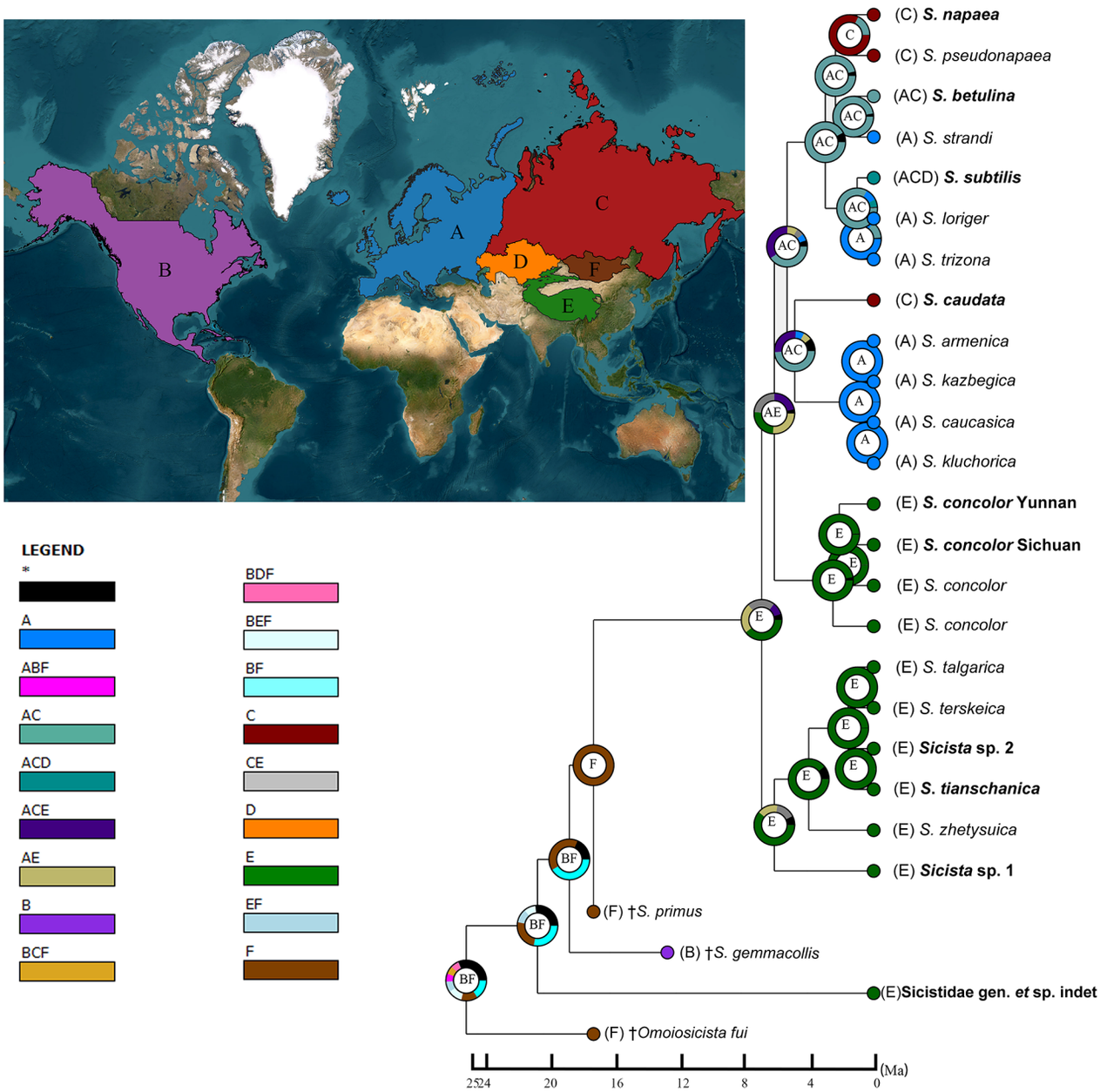

Figure 6 Ancestral range estimation using the BAYAREALIKE model

A: West Palearctic; B: Nearctic; C: Siberia, Far East and South-East Russia; D: Kazakh Steppe; E: Tibetan Plateau and surrounding mountains; F: "Gobi" (current Gobi Desert) and surrounding areas. Tip labels in bold indicate new specimens in this study.

Furthermore, incisive foramina facilitate the passage of the vomeronasal organ, which is crucial for pheromone-mediated communication, particularly during mating seasons (Wysocki et al., 1983; Wysocki & Lepri, 1991). Additional diagnostic features included a posterior palatal margin that extended medially beyond the M^3 posterior margins and molar characters such as a pronounced anterocone and a longitudinal ridge connecting the posteroloph to the metaloph in M^1 and M^2, consistent with established diagnostic features of Sicistidae (Li & Qiu, 2019). Geographically, Sicistidae gen. *et* sp. indet. was isolated from other *Sicista* spp. by the Yarlung Zangbo River, a significant biogeographic barrier. This lineage also possessed a longer hind foot compared to *Sicista*. Based on these morphological and molecular distinctions, this lineage is proposed as a new genus and species within the Sicistidae family: *Breviforamen shannanensis* **gen. *et* sp. nov.** A cyt *b* gene sequence (GenBank Accession: PQ227707) labeled as "*S. c. leathemi*" and collected in Xizang, China, formed a sister group to *Breviforamen shannanensis* **gen. *et* sp. nov.,** with a Kimura 2-parameter distance of 18.48% (Supplementary Table S10). However, no additional taxonomic data were available beyond the NCBI database record. Further field surveys across the East Himalayan region are needed to assess whether this sequence represents a second undescribed species within the new genus. No molecular data were available for true *S. c. leathemi* from Kashmir. However, photographic material of *S. c. flavus* (a junior synonym of *S. c. leathemi*) released by the National Museum of Natural History enabled comparative morphological evaluation. Features such as the extended incisive foramen, flared zygomatic arch, and anteroconid-protoconid connection in M_1 supported its placement within

Sicista. These observations suggest that *S. c. leathemi* may be more closely related to taxa from Central Asia than to *S. concolor*, especially considering the distinct position of *Breviforamen* **gen. nov.** them. Continued fieldwork in this region may uncover additional taxa, contributing to a more comprehensive understanding of Sicistidae evolution and diversification.

Molecular phylogenetic analyses supported *Sicista* sp. 1 as a monophyletic lineage at the base of the *tianschanica* species group (Figure 2), diverging from its sister clades approximately 6.04 Ma (Figure 5). Morphologically, *Sicista* sp. 1 differed markedly from other members of the *tianschanica* species group: (1) it had the shortest tail length and smallest body size (see Results); (2) it featured a uniquely black plantar surface, including the toes, compared to other species in the lineage (Supplementary Figure S3, Lebedev et al., 2021); (3) eight of the 11 individuals studied showed a yellow eye ring due to reduced black bristle-like hairs around the eyes. Among species lacking a dorsal stripe, *Sicista* sp. 1 was further distinguished by its unusually short tail. Based on these findings, *Sicista* sp. 1 is proposed as a new species within the genus *Sicista*: *Sicista brevicauda* **sp. nov.**

Although *Sicista* sp. 2 formed a distinct operational taxonomic unit (OTU) on the mitochondrial gene tree, it exhibited incongruent placement in the nuclear phylogeny, clustering with *S. tianschanica*. Morphologically, it resembled *S. tianschanica*, and no consistent diagnostic features were observed. Consequently, its taxonomic status could not be confirmed. Further molecular analyses are necessary to determine whether *Sicista* sp. 2 represents a case of incomplete lineage sorting, introgression.

New taxa description

Class Mammalia Linnaeus, 1758
Order Rodentia Bowdich, 1821
Suborder Myomorpha Brandt, 1855
Superfamily Dipodoidea Fischer von Waldheim, 1817
Family Sicistidae Allen, 1901

Breviforamen Zhu, Jiang, Li Q., *et* Chen., **gen. nov.**

ZooBank registration: urn:lsid:zoobank.org:act:FE8246C5-EE45-4A47-93B0-2FDDC54C86E7

Type species: *Breviforamen shannanensis* Zhu, Jiang, Li Q., *et* Chen, **sp. nov.**

Etymology: The generic name "*Breviforamen*" combines the Latin prefix "*brevis*", meaning short, with "foramen", meaning opening or perforation. It refers to the abbreviated incisive foramen, which is restricted to the anterior line connecting the premolars —a key diagnostic feature distinguishing it from extant *Sicista* species within Sicistidae. The genus name is of neuter gender.

Suggested common name: Short-foramen birch mouse (in English)/ duǎn kǒng jué shǔ (短孔蹶鼠属 in Chinese).

Diagnosis: Posterior margin of the palate extends medially, projecting well beyond the line connecting the posterior margins of the third upper molars. First (M^1) and second (M^2) upper molars exhibit prominent anterocones and distinct longitudinal ridges that connect the posteroloph to the metaloph. Incisive foramina are notably short, terminating anterior to the premolars. Posterior end of the nasal septum associated with the incisive foramina tapers gradually, without abrupt convergence. Upper molars lack an anterior cingulum. Auditory bulla opening presents a trapezoidal shape in ventral view (Figures 7, 8; Supplementary Figure S4). Tail is long, measuring between 134–148 mm, with long, white hairs. Hair length on the ventral side averages 3.56 mm (range: 3.23–3.91 mm, *n*=10), while hair on the dorsal side averages 1.51 mm (range: 1.26–1.84 mm, *n*=10) (Figure 8; Supplementary Figure S5). Hind foot is also elongated, measuring 23–24 mm.

Description: The genus is currently monotypic. The description follows that of *Breviforamen shannanensis* Zhu, Jiang, Li Q., *et* Chen, **sp. nov.** below.

Comparison: *Breviforamen* **gen. nov.** differs from the extant genus *Sicista* and fossil genus † *Omoiosicista* by its short incisive foramina, which do not extend to the anterior connecting line between the fourth premolars (P^4). It further differs from † *Omoiosicista* by the absence of an anterior cingulum on the upper molars. The new genus also exhibits a notably longer hind foot compared to *Sicista* (23–24 mm vs. 12–22 mm). The M_1 of *Breviforamen* **gen. nov.** bears an ectostylid and two distinct anteroconids, positioned centrally on the metalophid rather than adjacent to the metaconid or protoconid—together constituting a diagnostic combination not observed in *Sicista* (Figure 7; Supplementary Figure S6). Geographically, *Breviforamen* **gen. nov.** is restricted to the western side of the Yarlung Zangbo River in southern Xizang and represents the first documented member of Sicistidae, extant or fossil, from this region.

Breviforamen shannanensis Zhu, Jiang, Li Q., *et* Chen, **sp. nov.**

Suggested common name: Shannan short-foramen birch mouse (in English)/ Shān nán duǎn kǒng jué shǔ (山南短孔蹶鼠 in Chinese).

ZooBank registration: urn:lsid:zoobank.org:act:A86092ED-551C-454A-9CFC-796EB5C0E6CC

Holotype: KIZ 042965 (Field No. SN2023081130), ♂, collected by Changzhe Pu on 17 September 2023. Muscle tissue, skin specimen, and skull specimen are stored at the Kunming Natural History Museum of Zoology, Kunming Institute of Zoology, Chinese Academy of Sciences.

Type locality: Zhari Township, Longzi County, Shannan City, Xizang Autonomous Region, China (N28.701°, E93.178°) at 3 900 m above mean sea level (a.s.l.). (中国西藏自治区山南市隆子县扎日乡 in Chinese).

Etymology: The specific name "*shannanensis*" is derived from the name of the type locality, Shannan City, Xizang, China, combined with the Latin suffix "-*ensis*", meaning "belonging to".

Paratype: KIZ 042966 (Field No. SN2023081169), ♂, collected by Kang Luo on 18 September 2023 between 4 200 and 4 300 m a.s.l. Zhari Township, Longzi County, Shannan City, Xizang Autonomous Region, China (N28.712°; E93.098°). Muscle tissue, skin specimen, and skull specimen are stored at the Kunming Natural History Museum of Zoology, Kunming Institute of Zoology, Chinese Academy of Sciences.

Diagnosis: Same as the genus diagnosis (see above).

Description:

General appearance: A large-sized birch mouse distinguished by its long tail and hind foot. Measurements of the holotype include: head-body length of 80 mm, tail length of 148 mm, hind foot length of 24 mm, weight of 10.6 g, and ear length of 14 mm. Dorsal fur on the mid-back is blackish-gray, with individual hairs characterized by an ink-black base, saffron-yellow tips, and black bristles. Towards the sides, the fur

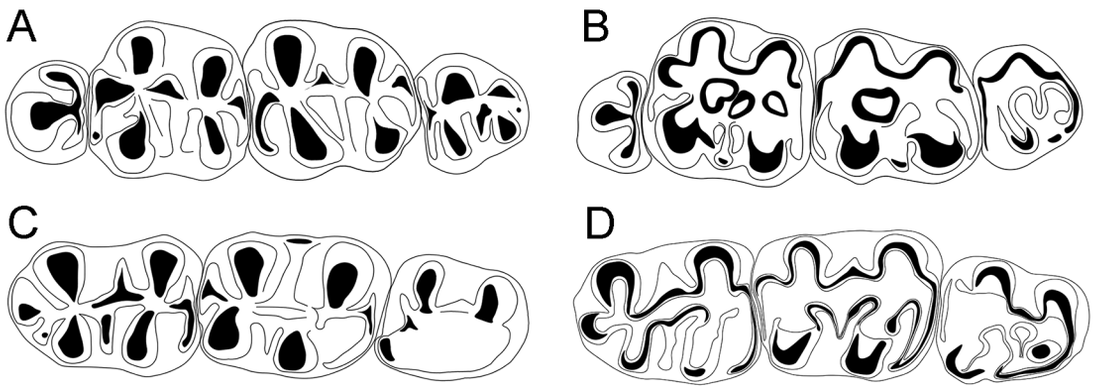

Figure 7 Buccal dentition patterns of *Breviforamen shannanensis* sp. nov. and *Sicista brevicauda* sp. nov.

A: Right upper dentition of *Breviforamen shannanensis* **sp. nov.** B: Right upper dentition of *Sicista brevicauda* **sp. nov.** C: Right lower dentition of *Breviforamen shannanensis* **sp. nov.** D: Right lower dentition of *Sicista brevicauda* **sp. nov.**

transitions to yellowish-gray, with a similar hair structure but denser bristling compared to the mid-back. Ventral pelage is ash-gray, with hairs featuring an ink-black base and primrose-yellow tips, lacking bristles. Boundary between the dorsal and ventral coloration is indistinct. Tail is distinctly bicolored: dorsal side is blackish-gray, with sparse hair that leaves the skin visible except for the final 7 mm, where the hair becomes denser and fully conceals the skin; ventral side is white, with denser and longer hair that obscures the skin except for the final 42 mm. Hair length measurements reveal significant variation between the dorsal and ventral surfaces: ventral hairs average 3.56 mm (range: 3.23–3.91 mm; *n*=10), while dorsal hairs average 1.51 mm (range: 1.26–1.84 mm; *n*=10). Field photos are presented in Supplementary Figure S7.

Skull: Skull is large, with a wide palate. Measurements of the holotype include: skull length of 21.69 mm and palatal width of 4.77 mm. Zygomatic arches converge anteriorly, reaching their widest point at the braincase. Palatal bone extends into a small cusp beyond the line of the third upper molar. Posterior edges of the incisive foramina are short, nearly reaching but not intersecting the anterior line connecting the premolars. Palatine foramen is positioned between the second and third upper molars. Posterior palate lacks transverse ridges.

Dentition: Dental formula of the species is 1.0.1.3/1.0.0.3, totaling 18 teeth (Figure 7). Incisors are smooth on the labial side, lack longitudinal grooves, and exhibit a yellow coloration. Molars have a cusp-ridge pattern with low crowns and high, sharp cusps. Upper molars lack an anterior cingulum, while upper premolars are single-rooted, and molars are three-rooted. P^4 is degenerate, subrounded, and characterized by a single cusp connected to a posterior ridge. M^1 is nearly square, with well-developed main cusps and an enlarged anterocone. It lacks enamel islands, and the mesosinus is open without a transverse crest. Mesoloph is closer to the middle of the entoloph but was absent in one of the two specimens examined. Metaloph is straight and connects to the center of the metacone, which is less compressed compared to *Sicista*. M^2 is rectangular, with well-developed main cusps and a weaker anterocone than M^1. Mesoloph is weak or absent, and hyposinus is present. Structures such as the anterocone, anteroloph, posterocone, and posteroloph are well-developed. M^3 is triangular and exhibits a pattern similar to M^1 and M^2, with all four main cusps present, although the hypocone is the smallest. Mesoloph is long, while anteroloph is well-developed on both lingual and buccal sides. Posterocone is weak or absent.

Lower molars are two-rooted. M_1 is rectangular, with well-developed main cusps. Anteroconid connects to the middle of protoconid and metalophid, and approximately half of the observed M_1 specimens exhibit two anteroconids. Protoconid is directed transversely, and anterior ectolophid connects to the metalophid near the metaconid. Ectostylid is present on both the buccal and lingual sides in half of the M_1 specimens. Mesolophid is long but weak and lower than the ectolophid. Arm of the entoconid extends posterolabially, with a longitudinal ridge between the posterolophid and hypoconid. Posteroconid is present, while no accessory cusp is present in the posterior fossette. M_2 has well-developed main cusps, a weaker anterocone than M_1, and a relatively forward metaconid compared to the protoconid. Arm of the entoconid extends posterolabially and connects to the hypoconid. Mesolophid is long. M_3 is rectangular, with the entoconid and anterocone absent. It also lacks the posterior arm of the protoconid and mesolophid.

Comparisons: Same as for the genus (see above).

Distribution: The species is currently known only from the type locality, Zhari Township, Longzi County, Shannan City, Xizang Autonomous Region, China, spanning an altitudinal range of 3 900–4 300 m a.s.l.

Ecology and habitat: The habitat of the type locality consisted of shrubs, rhododendron forests, and fir trees, distributed in high-altitude areas. Individuals were captured on the branches of rhododendron trees on the mountain slopes.

Genus *Sicista* Gray, 1827

Sicista brevicauda Zhu, Li Q., Chen *et* Jiang, **sp. nov.**

Suggested common name: Short-tailed birch mouse (in English)/ Duǎn wěi jué shǔ (短尾蹶鼠 in Chinese).

ZooBank registration: urn:lsid:zoobank.org:act:E88DB1DC-B0FC-40F8-AD66-54CDAA869F31

Holotype: KIZ 042967 (Field No. XTS2021138), ♀, collected by Kang Luo on 24 June 2021. Muscle tissue, skin specimen, and skull specimen are stored at the Kunming Natural History Museum of Zoology, Kunming Institute of Zoology, Chinese Academy of Sciences.

Type locality: Kurdening Nature Reserve, Mohuer Township, Gongliu County, Ili Kazakh Autonomous Prefecture, Xinjiang Uygur Autonomous Region, China (N43.149°, E82.898°), elevation approximately 1 750 m a.s.l. (中国新疆维吾尔自治区伊犁哈萨克自治州巩留县莫乎尔乡库尔德宁自然保护区 in

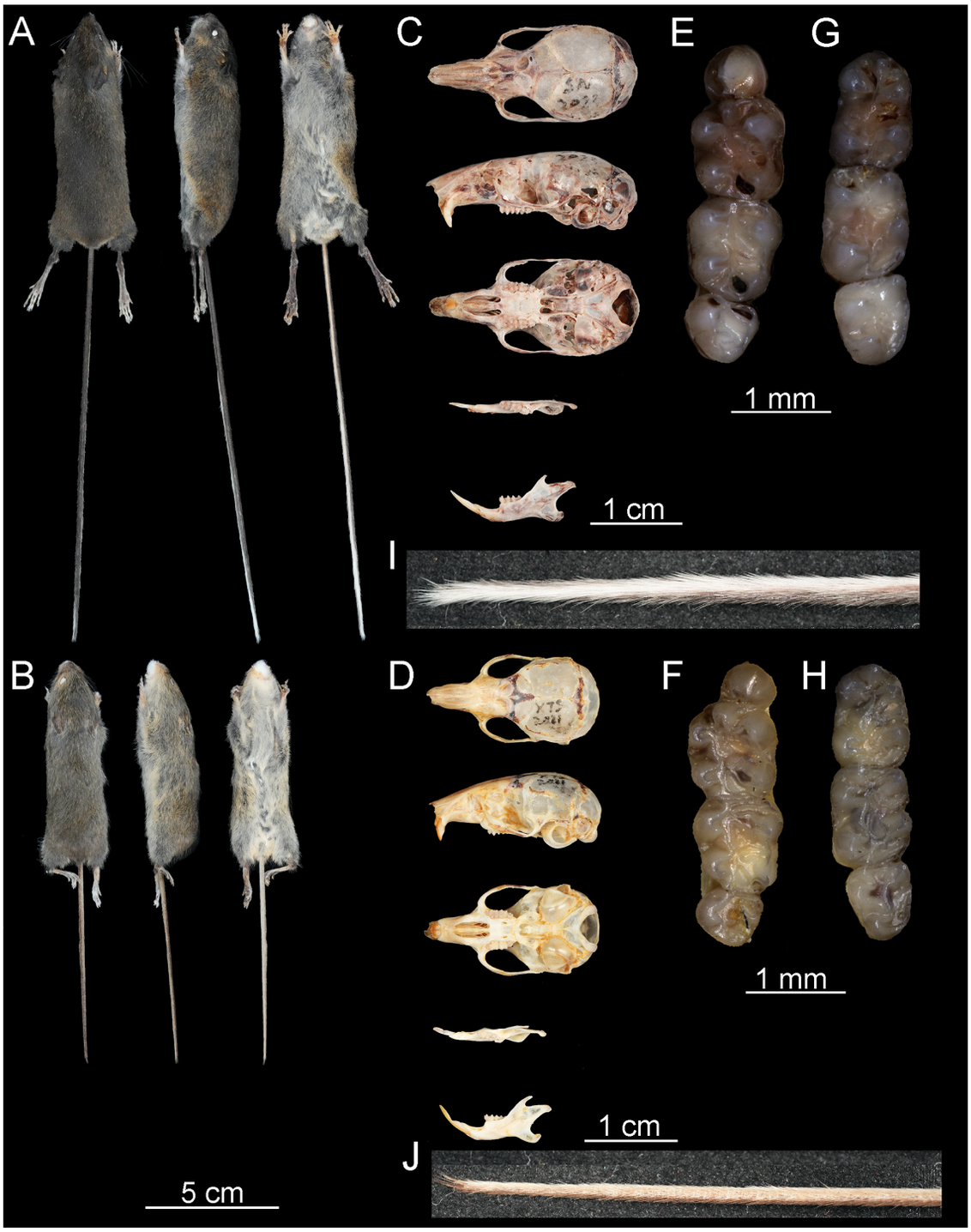

Figure 8 Comparative morphological features of *Breviforamen shannanensis* sp. nov. and *Sicista brevicauda* sp. nov.

A, B: Dorsal, lateral, and ventral views of the skins of *Breviforamen shannanensis* **sp. nov.** (Holotype, KIZ 042965, Field No. SN2023081130) (A) and *Sicista brevicauda* **sp. nov.** (Holotype, KIZ 042967, Field No. XTS2021138) (B). C, D: Dorsal, ventral, and lateral views of the skull and dorsal and lateral views of the mandible of *Breviforamen shannanensis* **sp. nov.** (C) and *Sicista brevi* **sp. nov.** (D). E–H: Upper and lower molar images of *Breviforamen shannanensis* **sp. nov.** (E and G) and *Sicista brevicauda* **sp. nov.** (F and H). I, J: Tail images of *Breviforamen shannanensis* **sp. nov.** (I) and *Sicista brevicauda* **sp. nov.** (J).

Chinese).

Etymology: The species name "*brevicauda*" is derived from the Latin "*brevis*", meaning short, and "cauda", meaning tail, referring to the distinctly short tail characteristic of this birch mouse species.

Paratype: KIZ 042968 (Field No. XTS2021017), ♀, collected by Kang Luo on 21 June 2021 and KIZ 042969 (Field No. XTS2021026), ♂, collected by Jing Luo on 21 June 2021. Individuals were collected in Kurdening Nature Reserve, Mohuer Township, Gongliu County, Ili Kazakh Autonomous Prefecture, Xinjiang Uygur Autonomous Region, China (N43.171°, E82.880°) at 1 423 m a.s.l. Muscle tissue, skin specimen, and skull specimen are stored at the Kunming Natural History Museum of Zoology, Kunming Institute of Zoology, Chinese Academy of Sciences.

Specimens examined: KIZ 042974 (Field No. HJ202407095),

♂; KIZ 042976 (Field No. HJ202407096), ♀; KIZ 042975 (Field No. HJ202407109), ♂; KIZ 042971 (Field No. HJ202407128), ♀; KIZ 042972 (Field No. HJ202407129), ♂; KIZ 042973 (Field No. HJ202407147), ♂; KIZ 042970 (Field No. HJ202407173), ♀; KIZ 042977 (Field No. HJ202407176), ♂, collected by Jing Luo and Mingjin Pu in July 2024. Individuals were collected in Bayinbuluk Scenic Area and Swan Lake Scenic Area, Bayingolin Township, Hejing County, Bayingolin Mongolian Autonomous Prefecture, Xinjiang Uygur Autonomous Region, China (N42.704°; E83.753°) ranging from 2 495 to 2 555 m a.s.l. Muscle tissue, skin specimen, and skull specimen are stored at the Kunming Institute of Zoology, Chinese Academy of Sciences.

Diagnosis: A small-bodied *Sicista* species (65±4.33 mm, 60–70 mm) characterized by the absence of dorsal stripes and a distinctly short tail (mean=73.38 mm, range=68–76 mm). A yellow eye ring is present in 72% of individuals. Plantar surfaces of the forefeet are uniformly black.

Description:

General appearance: Sicista brevicauda **sp. nov.** is a small-sized birch mouse with a notably short tail. Measurements of the holotype include: head-body length of 65 mm, tail length of 75 mm, hind foot length of 15 mm, weight of 8.6 g, and ear length of 12 mm. Dorsal pelage is wax yellow, with individual hairs characterized by an ink-black base, sulfur-yellow tips, and black bristles. Ventral pelage is primrose yellow, with hairs featuring an ink-black base and primrose-yellow tips, lacking bristles. Boundary between the dorsal and ventral pelage is indistinct. Tail is indistinctly bicolored, with the dorsal side being wax yellow and ventral side being yellowish gray. In both cases, the hair is sparse, making the skin visible along the entire tail. Hair length measurements on the ventral side average 1.67 mm (range: 1.49–1.75 mm; *n*=10), while dorsal hairs average 1.25 mm (range: 1.07–1.55 mm; *n*=10). Field photos are presented in Supplementary Figure S8.

Skull: Skull is relatively small, measuring 18.6 mm in length, with slightly outward zygomatic arches that are widest at the arches themselves. Palatal bone extends into a small cusp beyond the line of the third upper molar. Palatine foramen is positioned at the second upper molar, and the posterior palate displays distinct transverse ridges.

Dentition: Dental formula of the new species is 1.0.1.3/1.0.0.3= 18 (Figure 7). Incisors have a smooth labial surface and are orange-yellow in color. Upper premolars (one-rooted) and molars (three-rooted) show distinct occlusal patterns: P^4 is degenerate and subrounded, with a single cusp connected to a posterior ridge; M^1 is nearly square, with well-developed main cusps, an enlarged and “squashed” anterocone, and three enamel islands in about one-third of specimens. In M^1, the anterior arm of the protocone is nearly absent, the mesosinus is open without a transverse crest, the mesoloph lies near the middle of the entoloph, and the metacone is square and flattened. M^2 is rectangular, with well-developed main cusps, a weak or absent mesoloph, and an indistinct hyposinus; although the anteroloph and posteroloph are present, the anterocone and posterocone are absent. M^3 is triangular, bearing only the paracone and protocone of the four main cusps, with a short or absent mesoloph, a well-developed anteroloph on the lingual side, and anterocone and posterocone both absent.

Lower molars (two-rooted) are rectangular with well-developed main cusps. In M_1, the anteroconid connects to the protoconid, the protoconid is transversely extended, and the anterior ectolophid meets the metalophid. There is no mesostylid on the labial side, and although the mesolophid is long, it is lower than the ectolophid; the arm of the entoconid extends posterolabially, and a longitudinal ridge between the posterolophid and hypoconid is present, with no posteroconid or accessory cusp in the posterior fossette. M_2 is rectangular, with a weaker anterocone than in M_1, and a metaconid located farther forward relative to the protoconid; the arm of the entoconid is absent, and the mesolophid is either absent or conspicuously long. M_3 is rectangular, lacking a visible entoconid and the posterior arm of the protoconid and mesolophid.

Comparison: *Sicista brevicauda* **sp. nov.** can be readily distinguished from *S. subtilis*, *S. betulina*, *S. strandi*, *S. loriger*, and *S. trizona* by the absence of a dorsal stripe. Among the unstriped *Sicista* species, *Sicista brevicauda* **sp. nov.** has a significantly shorter tail (73.38±2.62 mm, range: 69–76 mm) compared to other *Sicista* species: *S. caudata* (111.4 mm, range: 99.4–118.2 mm), *S. caucasica* (95.5 mm, range: 84–105.8 mm), *S. kluchorica* (98.6 mm, range: 86.4–107.5 mm), *S. kazbegica* (102 mm, range: 94.5–109.5 mm), *S. armenica* (98.4 mm, range: 95.5–101.5 mm), *S. zhetysuica* (98.3 mm, range: 91–110 mm), *S. talgarica* (106.4 mm, range: 102–113 mm), *S. terskeica* (94.1 mm, range: 85.7–103 mm), *S. tianschanica* (116.3 mm, range: 112–124 mm), *S. concolor* (135.67 mm, range: 126–150 mm), *S. pseudonapaea* (87.6 mm, range: 81.5–95 mm), and *S. napaea* (92.2 mm, range: 82.1–103 mm). The new species is geographically restricted to the West Tianshan Mountains of Xinjiang. It is distinguished by uniformly black plantar surfaces on the forefeet and the presence of a yellow eye ring (72% of individuals), features that differentiate it from other species within the *S. tianschanica* group (Supplementary Figures S3, S8).

Distribution: *Sicista brevicauda* **sp. nov.** is found in the West Tianshan Mountains at altitudes ranging from 1 423 to 1 750 m a.s.l. in the Kurdening Nature Reserve, Mohuer Township, Gongliu County, Ili Kazakh Autonomous Prefecture and at altitudes ranging from 2 495 to 2 555 m a.s.l. in the Bayinbuluk Scenic Area and Swan Lake Scenic Area, Bayingolin Township, Hejing County, Bayingolin Mongolian Autonomous Prefecture, Xinjiang Uygur Autonomous Region, China.

Ecology and habitat: The three specimens collected from Kurdening were found in mid-altitude montane environments dominated by mixed forests, grasslands, and fir trees, while the eight specimens collected from Bayingolin were associated with shrub-dominated landscapes in high elevations, with grazing activities observed in the surrounding areas.

Evolutionary significance of new lineages for Sicistidae

Breviforamen **gen. nov.** represents an ancient extant lineage within Sicistidae that originated in the Early Miocene (20.38 Ma), with a biogeographic range extending into the eastern Himalayas, a region not previously associated with the distribution of Sicistidae. This finding suggests an alternative scenario for the early dispersal or diversification of this family. During the emergence of this lineage, the Himalayas had already reached elevations of approximately 2 500 m a.s.l., a stage of orogenesis not yet associated with aridification in Central Asia (Favre et al., 2015; Zhu et al., 2022). Although birch mice are typically adapted to high-altitude habitats, *Breviforamen shannanensis* **gen. *et* sp. nov.** was recorded at

an altitude of 4 300 m a.s.l., the highest known elevation for any Sicistidae species, exceeding the previously reported record of 4 027 m a.s.l. for *S. concolor* (Holden et al., 2017). Remarkably, both specimens of *Breviforamen shannanensis* **sp. nov.** were captured in trees, approximately 4 m above the ground, whereas all 119 co-occurring individuals of shrews, rodents, and pikas were captured on the ground. Unlike typical *Sicista* spp., which are ground-dwelling usually (Cserkész et al., 2017; Lebedev et al., 2021; Shenbrot et al., 2008), *Breviforamen shannanensis* **sp. nov.** appears to exhibit arboreal tendencies, similar to *S. caudata* (Piao, 2019). Morphological traits such as an elongated hind foot and long tail, often associated with climbing and arborealism, support this interpretation. These adaptations, including elongated digits, are also seen in other arboreal species such as *Sylvisorex megalura* and *Soriculus leucops* (Hutterer, 1985), and are widely considered adaptations to climbing (Nations et al., 2019). They also facilitate jumping, a behavior hypothesized to have evolved in forested environments for predator avoidance and ecological expansion (McGowan & Collins, 2018; Wu et al., 2014), as exemplified by *Typhlomys chapensis*, which has been observed leaping between branches (Panyutina et al., 2017).

The apomorphic traits of *Breviforamen* **gen. nov.** include a P^4 cusp connected to a posterior ridge, an M_1 anteroconid attached to the metalophid, and a symmetrical arrangement of cusps on the upper molars. Unlike *Sicista*, where molar cusps are often compressed, *Breviforamen* **gen. nov.** retains four discernible cusps on M^3, though some are faint. These features resemble conditions observed in ancient taxa such as † *Heosminthus chimidae* from the Late Eocene (Li & Qiu, 2019). The same pattern occurs in its sister group: the anterior cingulum of M^1 in †*Omoiosicista fui*, which is prevalent in older taxa such as † *Heosminthus chimidae* (Early Oligocene–Miocene transition) and † *Litodonomys lajeensis* (Late Oligocene–Early Miocene) (Daxner-Höck et al., 2014). Additionally, the incisive foramina in *Breviforamen* **gen**. **nov**. are both short and broad—a configuration not seen in other sicistines, where short foramina tend to be narrow (Calede et al., 2022). Phylogenetic analyses based on both molecular and morphological datasets yielded consistent results, potentially reflecting limited morphological divergence within Sicistidae and long-term ecological stability in the eastern Himalaya forests, which may have preserved distinct ancestral traits (Chen et al., 2021b).

Additional diversity within *Breviforamen* **gen. nov.** in southern Xizang is also suggested by a mitochondrial cyt *b* sequence (GenBank ID: PQ227707), labeled as "*S. c. leathemi*," which formed a monophyletic group with *Breviforamen* **gen. nov.** rather than with *Sicista*. The Kimura 2-parameter distance between "*S. c. leathemi*" and *Breviforamen shannanensis* **gen. *et* sp. nov.** (18.48%) is considered significant for species-level differentiation (Rusin et al., 2018), suggesting that the eastern Himalayas have facilitated diversification within *Breviforamen* **gen. nov.**, paralleling the role of mountain systems in shaping speciation patterns within *Sicista*, as observed in the *caucasica* and *tianschanica* species groups.

The discovery of *Breviforamen shannanensis* **sp. nov.** provides a critical phylogenetic link between ancient fossil taxa and extant Sicistidae, markedly expanding the known diversity of the family. This finding highlights the influence of Himalayan geological processes on the dispersal and diversification of ancient taxa and the function of the region as a long-term refugium. Divergence times among terrestrial vertebrates correspond closely with regional tectonic events. For example, molecular divergence within the *tianschanica* species group spanned from 6.04 to 0.99 Ma, aligning with the prolonged uplift of the Tianshan Mountains between 7 and 2.58 Ma during the early Pleistocene. Similarly, the short divergence history within the *caucasica* species group (1.16–0.57 Ma) mirrors the rapid uplift of the Caucasus range during the same period (Rusin et al., 2018; Sun et al., 2004).

Diversification and dispersal of Sicistidae

Total evidence tip-and-node dating estimated the divergence of *Breviforamen shannanensis* **gen. *et* sp. nov.** at 20.38 Ma (95% CI: 17.40–24.02 Ma), preceding the earliest known fossil records of *Sicista* spp. (16–20 Ma) (Wang et al., 2009). This supports the view that divergence typically predates the appearance of corresponding fossil evidence (Chen et al., 2021a). Zhang et al. (2013) proposed that the warm climatic conditions during the late Oligocene to early Miocene promoted the early diversification and dispersal of Sicistidae, facilitating the emergence of genus-level diversity. During this interval, Dipodidae accounted for 31% of rodent fossils in the Gashunyinadege Fauna (Kimura, 2010), while palynological data indicate that northern China was dominated by deciduous broadleaf forests (Zhao et al., 2018). Concurrently, the Yarlung Zangbo River emerged but had not yet established a north-south biogeographic barrier (Song et al., 2021), and the Himalayas had only recently attained elevations near 2 500 m a.s.l. (Zhu et al., 2022). These environmental and geological transitions likely contributed to the early radiation and geographic dispersal of Sicistidae.

Ancestral range reconstruction indicated that the "Gobi" region and North America were the two most likely centers of origin for both Sicistidae and *Breviforamen* **gen. nov.**, although the precise sites remain undetermined due to closely matched probabilities ("Gobi": 15.96%; "Gobi" + North America: 13.14%). Throughout most of the Cenozoic era, the Bering Strait remained closed until the Late Miocene (5.32 Ma) (Gladenkov et al., 2002), enabling faunal exchange between Eurasia and the Americas. The present ancestral distribution analysis supports intercontinental dispersal within *Sicista*, aligning with earlier suggestions that †*S. gemmacollis* dispersed from Asia to North America, while contradicting the hypothesis that Chinese *Sicista* originated in the Americas (Kimura, 2013), instead favoring an Asian origin. This contradiction arises because the view proposed by Kimura (2013) preceded the description of †*S. ertemteensis* by Qiu and Li (2016), which led to the inference that †*S. gemmacollis* from North America represented the second oldest *Sicista* lineage. Subsequent fossil evidence from the "Gobi" region demonstrated that †*S. ertemteensis* is contemporaneous with † *S. gemmacollis* (Green, 1977; Qiu & Li, 2016), thereby supporting an Asian rather than American origin, consistent with the present results. Furthermore, the peak in intercontinental mammalian dispersal during the Oligocene–Miocene period (Jiang et al., 2019) and accumulating evidence from fossil and extant *Sicista* species support East Asia as the more likely center of origin of the genus (Cserkész et al., 2019; Kimura, 2013; Pisano et al., 2015). In this context, the diversification of Sicistidae into † *Omoiosicista*, *Sicista*, and *Breviforamen* **gen. nov**. likely occurred during the late Oligocene to early Miocene under

warm climatic conditions, with extensive deciduous broadleaf forests across the "Gobi" region and into North America (Reichgelt et al., 2023; Zhao et al., 2018). Subsequent mid-Miocene global cooling (Zachos et al., 2001), combined with increasing aridity across interior Asia (Guo et al., 2002), was likely intensified by tectonic uplift of the Qinghai-Xizang Plateau and Himalayas (Favre et al., 2015; Lu et al., 2019). These changes may have led to the extinction of †*Omoiosicista* and †*S. primus*, the trans-Beringian dispersal of early *Sicista* to North America, and the southward migration of *Breviforamen* **gen. nov**. into what is now southern Xizang. Our ancestral distribution reconstruction for *Breviforamen shannanensis* **sp. nov.** supports a northern origin, extending from the "Gobi" region into North America. Environmental degradation following the mid-Miocene may have driven its migration southward to the Himalayan region, where it now occupies azalea-dominated montane forests between 3 900–4 300 m a.s.l.. Palynological records from the Gyirong Basin suggest that the region supported mixed coniferous and broadleaf forests during the middle Miocene (Liu et al., 2024), providing a favorable habitat for forest-adapted taxa such as *Breviforamen* **gen. nov.** The presence of this ancient lineage in southern Xizang reveals a previously unrecognized dispersal route within Sicistidae. The formation of the Yarlung Zangbo River, initiated in the Early Miocene and completed by the Late Miocene (Song et al., 2021), also sheds light on the origins and dispersal of *Breviforamen* **gen. nov.**, suggesting migration into southern Xizang during the middle to late Miocene. Similar north-to-south Miocene migration patterns have been observed in other small mammals such as *Alpiscaptulus medogensis* (Chen et al., 2021b) and flying squirrels (Lu et al., 2013). Broader biogeographic investigations across diverse mammalian groups are essential to further elucidate the origins, diversification, and evolutionary trajectories of Himalayan fauna.

Previous phylogenetic reconstructions identified the "*tianschanica*" lineage as the most basal within the genus *Sicista*, followed by the "*concolor*" lineage with moderate support, largely due to inadequate taxonomic sampling (Cserkész et al., 2019; Lebedev et al., 2019; Pisano et al., 2015). The present study corroborates this phylogenetic framework with additional specimens from Sichuan and Yunnan, China. However, conflicting interpretations persist regarding the recent habitat shifts in *Sicista*. While Cserkész et al. (2019) proposed a recent transition from montane to lowland environments, Lebedev et al. (2019) proposed the opposite pattern. The current findings support the hypothesis of a shift from lowlands to mountains.

During the late middle Miocene, *Sicista* re-colonized the "Gobi" region, as evidenced by the appearance of † *S. ertemteensis*, followed by subsequent records of † *S. bilikeensis* and † *S. wangi* from the late Miocene to Early Pliocene (Li & Qiu, 2019). Concurrently, *Sicista* fossils from the Late Miocene have also been recovered from lowland and plain regions in Kazakhstan (Savinov, 1970; Sinitsa et al., 2024). The last occurrence of *Sicista* in the "Gobi" region dates to the early Pliocene, a period that coincides closely with the Pliocene–Pleistocene climatic transition. These events suggest that *Sicista* populations in China migrated from the "Gobi" region to higher elevations, including the Tianshan Mountains and southeastern margins of the Xizang Plateau. The common ancestor of the "*caucasica*" and "*caudata*" lineages appears to have been broadly distributed across Eurasia, although these groups are currently isolated in two distant geographic regions: the "*caucasica*" lineage is restricted to the Caucasus Mountains, while the "*caudata*" lineage is confined to far eastern Russia and northeastern China (Lebedev et al., 2019; Shenbrot et al., 2008). Notably, fossil evidence is lacking from montane areas of the Tianshan and Hengduanshan regions during the Late Miocene to Pliocene in China (Li & Qiu, 2019). Following extinction and migration events after the Middle Miocene Climatic Optimum, *Sicista* re-colonized the "Gobi" region during the late middle Miocene, yet exhibited limited diversification, as only one species, † *S. ertemteensis*, is known from this interval—likely reflecting the suppressive effects of global cooling (Zachos et al., 2001). Diversification resumed in the late Miocene, marked by a rise in fossil species diversity and the molecular divergence of the "*tianschanica*" and "*concolor*" lineages. In contrast to the widespread aridification across global mid-latitudes during this period, northern China experienced increased humidity, which may have facilitated the rapid divergence of *Sicista* (Fortelius & Zhang, 2006). By the late Pliocene, with the formation of the modern Gobi Desert driven by declining humidity and cooling, extant *Sicista* species began ascending to montane habitats (Lu et al., 2019). Climatic fluctuations during the Pliocene–Pleistocene further promoted their migration to mountain systems across Eurasia (Lebedev et al., 2019). Of note, both fossil and extant members of Sicistidae are found along the mountainous edges of the Qinghai-Xizang Plateau. This distribution pattern likely reflects the transformation of Qinghai-Xizang Plateau, which initially featured a warm, humid central valley between 50 and 38 Ma. Subsequent uplift between approximately 38 and 29 Ma altered the region into a colder and drier environment, predating the emergence of Sicistidae (Xiong et al., 2022). Together, these findings suggest that birch mice are more dependent on humid environments than other dipodoids such as jerboas. Warm and humid climates promote diversification in *Sicista*, while arid environments are associated with extinction, reduced diversity, and migration.

SCIENTIFIC FIELD SURVEY PERMISSION INFORMATION

Permission for field surveys in Xizang Autonomous Region, China, was granted by the Xizang Autonomous Region Forestry and Grassland Bureau. Permission for field surveys in Xinjiang Uygur Autonomous Region, China, was granted by the Ili Kazakh Autonomous Prefecture Forestry and Grassland Bureau. Permission for field surveys in Sichuan Province, China, was granted by the Songpan County Forestry and Grassland Bureau. Permission for field surveys in Yunnan Province, China, was granted by the Deqin Sub-bureau of the Baima Snow Mountain National Nature Reserve.

SUPPLEMENTARY DATA

Supplementary data to this article can be found online.

COMPETING INTERESTS

The authors declare that they have no competing interests.

AUTHORS' CONTRIBUTIONS

Z.X.Z.: Data generation and analyses, manuscript writing and revision. Q.L.: Morphological analyses, manuscript writing and revision. W.Y.S.: Specimen collection, manuscript writing and revision. X.Y.L.: Manuscript review and editing. M.Y.W.: Field work and coordination. X.X.P.: Manuscript revision. K.L., J.L., M.J.P., and C.Z.P.: Specimen collection. H.J.W.: Data compilation. A.L. and Z.L.: Tissue samples provision. Z.Z.C.: Molecular results review, manuscript review and editing. X.L.J.: Study design,

manuscript review and editing. All authors read and approved the final version of the manuscript.

ACKNOWLEDGMENTS

Many thanks are given to the Administration of Forestry and Grassland of Xizang, Xinjiang, Yunnan and Sichuan Province for their permission to conduct field work. We also thank Professor Wei-Kang Yang (Xinjiang Institute of Ecology and Geography, Chinese Academy of Sciences) for coordination and support during fieldwork in Xinjiang. We are also grateful to the National Animal Collection Resource Center (NACRC), China, for allowing us to examine their specimens, as well as to the United States National Museum of Natural History and the Siberian Branch of the Russian Academy of Sciences (Novosibirsk, Russia).

REFERENCES

Baele G, Lemey P, Bedford T, et al. 2012. Improving the accuracy of demographic and molecular clock model comparison while accommodating phylogenetic uncertainty. *Molecular Biology and Evolution*, **29**(9): 2157–2167.

Bouckaert R, Heled J, Kühnert D, et al. 2014. BEAST 2: a software platform for Bayesian evolutionary analysis. *PLoS Computational Biology*, **10**(4): e1003537.

Calede JJM, Tse YT, Cairns KD. 2022. The first evidence of *Heosminthus* from North America and the phylogenetics of Sminthidae (Mammalia, Rodentia, Dipodoidea): biogeographical implications. *Journal of Systematic Palaeontology*, **20**(1): 1–21.

Camacho-Sanchez M, Leonard JA. 2020. Mitogenomes reveal multiple colonization of mountains by *Rattus* in Sundaland. *Journal of Heredity*, **111**(4): 392–404.

Chen YK, Wang Y, Li JL, et al. 2021a. Principles, error sources and application suggestions of prevailing molecular dating methods. *Biodiversity Science*, **29**(5): 629–646. (in Chinese).

Chen ZZ, He SW, Hu WH, et al. 2021b. Morphology and phylogeny of scalopine moles (Eulipotyphla: Talpidae: Scalopini) from the eastern Himalayas, with descriptions of a new genus and species. *Zoological Journal of the Linnean Society*, **193**(2): 432–444.

Cheng JL, Xia L, Wen ZX, et al. 2021. Review on the systematic taxonomy of Dipodoidea in China. *Acta Theriologica Sinica*, **41**(3): 275–283. (in Chinese).

Cserkész T, Fülöp A, Almerekova S, et al. 2019. Phylogenetic and morphological analysis of birch mice (genus *Sicista*, family sminthidae, rodentia) in the Kazak cradle with description of a new species. *Journal of Mammalian Evolution*, **26**(1): 147–163.

Cserkész T, Rusin M, Czabán D, et al. 2017. Recent geographic distribution of birch mice (genus *Sicista*) in the western Great Caucasus Mts. , with designation of terra typica for *Sicista caucasica* (Sminthidae, Rodentia). *North-Western Journal of Zoology*, **13**(2): 371–375.

Cserkész T, Rusin M, Sramkó G. 2016. An integrative systematic revision of the European southern birch mice (Rodentia: Sminthidae, *Sicista subtilis* group). *Mammal Review*, **46**(2): 114–130.

Daxner-Höck G, Badamgrav D, Maridet O. 2014. Dipodidae (Rodentia, Mammalia) from the Oligocene and early Miocene of Mongolia. *Annalen des Naturhistorischen Museums in Wien, Serie A*, **116**: 131–214.

dos Reis M, Thawornwattana Y, Angelis K, et al. 2015. Uncertainty in the timing of origin of animals and the limits of precision in molecular timescales. *Current Biology*, **25**(22): 2939–2950.

Ellerman JR, Morrison-Scott TCS. 1951. Checklist of Palaearctic and Indian Mammals 1758 to 1946. London: Trustees of the British Museum (Natural History), 522–523.

Faurby S, Silvestro D, Werdelin L, et al. 2024. Reliable biogeography requires fossils: insights from a new species-level phylogeny of extinct and living carnivores. *Proceedings of the Royal Society B: Biological Sciences*, **291**(2028): 20240473.

Favre A, Päckert M, Pauls SU, et al. 2015. The role of the uplift of the Qinghai-Tibetan Plateau for the evolution of Tibetan biotas. *Biological Reviews*, **90**(1): 236–253.

Fortelius M, Zhang ZQ. 2006. An oasis in the desert? History of endemism and climate in the Late Neogene of North China. *Palaeontographica Abteilung A*, **277**(1): 131–141.

Giribet G. 2015. Morphology should not be forgotten in the era of genomics–a phylogenetic perspective. *Zoologischer Anzeiger - A Journal of Comparative Zoology*, **256**: 96–103.

Gladenkov AY, Oleinik AE, Marincovich Jr L, et al. 2002. A refined age for the earliest opening of Bering Strait. *Palaeogeography, Palaeoclimatology, Palaeoecology*, **183**(3–4): 321–328.

Green M. 1977. Neogene zapodidae (Mammalia: Rodentia) from South Dakota. *Journal of Paleontology*, **51**(5): 996–1015.

Guo ZT, Ruddiman WF, Hao QZ, et al. 2002. Onset of Asian desertification by 22 Myr ago inferred from loess deposits in China. *Nature*, **416**(6877): 159–163.

Hall ER. 1930. Rodents and Lagomorphs from the Later Tertiary of Fish Lake Valley, Nevada. Berkeley: University of California Press, 295–312.

Holden M, Musser G. 2005. Family dipodidae. *In*: Wilson DE, Reeder DM. Mammal Species of the World: A Taxonomic and Geographic Reference. 3rd ed. Baltimore: The Johns Hopkins University Press, 871–893.

Holden ME, Cserkész T, Musser G. 2017. Family sminthidae. *In*: Wilson DE, Lacher Jr TE, Mittermeier RA. Handbook of the Mammals of the World. Barcelona: Lynx Ediciones, 22–48.

Huelsenbeck JP, Rannala B. 2004. Frequentist properties of Bayesian posterior probabilities of phylogenetic trees under simple and complex substitution models. *Systematic Biology*, **53**(6): 904–913.

Hutterer R. 1985. Anatomical adaptations of shrews. *Mammal Review*, **15**(1): 43–55.

IUCN. 2024. The IUCN red list of threatened species. Version 2024-2. https://www.iucnredlist.org.

Jaeger JJ, Tong H, Denys C. 1986. The age of the *Mus-Rattus* divergence: paleontological data compared with the molecular clock. *Comptes Rendus De l'Academie Des Sciences Serie Ii*, **302**(14): 917–922.

Jiang DC, Klaus S, Zhang YP, et al. 2019. Asymmetric biotic interchange across the Bering land bridge between Eurasia and North America. *National Science Review*, **6**(4): 739–745.

Kimura Y. 2010. New material of dipodid rodents (Dipodidae, Rodentia) from the early Miocene of Gashunyinadege, Nei Mongol, China. *Journal of Vertebrate Paleontology*, **30**(6): 1860–1873.

Kimura Y. 2011. The earliest record of birch mice from the Early Miocene Nei Mongol, China. *Naturwissenschaften*, **98**(1): 87–95.

Kimura Y. 2013. Intercontinental dispersals of sminthid rodents (Sminthidae, Dipodidae, Rodentia) between Eurasia and North America. *In*: Wang X, Flynn LJ, Fortelius M. Fossil Mammals of Asia: Neogene Biostratigraphy and Chronology. New York: Columbia University Press, 656–675.

Kimura Y, Hawkins MTR, McDonough MM, et al. 2015. Corrected placement of *Mus-Rattus* fossil calibration forces precision in the molecular tree of rodents. *Scientific Reports*, **5**: 14444.

Lanfear R, Calcott B, Ho SYW, et al. 2012. Partitionfinder: combined selection of partitioning schemes and substitution models for phylogenetic analyses. *Molecular Biology and Evolution*, **29**(6): 1695–1701.

Lebedev VS, Bannikova AA, Pagès M, et al. 2013. Molecular phylogeny and systematics of Dipodoidea: a test of morphology-based hypotheses. *Zoologica Scripta*, **42**(3): 231–249.

Lebedev VS, Kovalskaya Y, Solovyeva EN, et al. 2021. Molecular systematics of the *Sicista tianschanica* species complex: a contribution from

historical DNA analysis. *PeerJ*, **9**: e10759.

Lebedev VS, Rusin MY, Zemlemerova ED, et al. 2019. Phylogeny and evolutionary history of birch mice *Sicista* Griffith, 1827 (Sminthidae, Rodentia): implications from a multigene study. *Journal of Zoological Systematics and Evolutionary Research*, **57**(3): 695–709.

Lewis PO. 2001. A likelihood approach to estimating phylogeny from discrete morphological character data. *Systematic Biology*, **50**(6): 913–925.

Li CK, Qiu ZD. 2019. Glires Ⅱ: Rodentia Ⅰ. *In*: Palaeovertebrata Sinica Volume III Basal Synapsids and Mammals Fascicle 5(1)(Serial no. 18-1). Beijing: Science Press. (in Chinese)

Li Q, Meng J. 2010. Erlianomys combinatus, a primitive myodont rodent from the Eocene Arshanto Formation, Nuhetingboerhe, Nei Mongol, China. *Vertebrata Palasiatica*, **48**(2): 133–144.

Liu J, Song A, Zhang XW, et al. 2024. Palynological assemblages and paleoenvironmental evolution in the Gyirong Basin since Middle Miocene. *Acta Petrologica Sinica*, **40**(5): 1418–1428. (in Chinese).

Lu HY, Wang XY, Wang XY, et al. 2019. Formation and evolution of Gobi Desert in central and eastern Asia. *Earth-Science Reviews*, **194**: 251–263.

Lu XF, Ge DY, Xia L, et al. 2013. The evolution and paleobiogeography of flying squirrels (Sciuridae, Pteromyini) in response to global environmental change. *Evolutionary Biology*, **40**(1): 117–132.

Luo AR, Zhang C, Zhu CD. 2021. Using BEAST 2 for Bayesian tip dating. *Bio-101*, e1010617. (in Chinese).

Massana KA, Beaulieu JM, Matzke NJ, et al. 2015. Non-null effects of the null range in biogeographic models: exploring parameter estimation in the DEC model. *BioRxiv*, doi: https://doi.org/10.1101/026914.

Matzke NJ. 2013. Probabilistic historical biogeography: new models for founder-event speciation, imperfect detection, and fossils allow improved accuracy and model-testing. *Frontiers of Biogeography*, **5**(4): 242–248.

Matzke NJ. 2014a. BioGeoBEARS: BioGeography with Bayesian (and Likelihood) evolutionary analysis in R Scripts. https://rdrr.io/cran/BioGeoBEARS/.

Matzke NJ. 2014b. Model selection in historical biogeography reveals that founder-event speciation is a crucial process in Island Clades. *Systematic Biology*, **63**(6): 951–970.

McGowan CP, Collins CE. 2018. Why do mammals hop? Understanding the ecology, biomechanics and evolution of bipedal hopping. *Journal of Experimental Biology*, **221**(12): jeb161661.

Minh B, Trifinopoulos J, Schrempf D, et al. 2018. IQ-TREE version 1.6. 8: Tutorials and Manual. Phylogenomic software by maximum likelihood. http://www.iqtree.org.

Minh BQ, Schmidt HA, Chernomor O, et al. 2020. IQ-TREE 2: new models and efficient methods for phylogenetic inference in the genomic era. *Molecular Biology and Evolution*, **37**(5): 1530–1534.

Nations JA, Heaney LR, Demos TC, et al. 2019. A simple skeletal measurement effectively predicts climbing behaviour in a diverse clade of small mammals. *Biological Journal of the Linnean Society*, **128**(2): 323–336.

O'Reilly JE, Donoghue PCJ. 2016. Tips and nodes are complementary not competing approaches to the calibration of molecular clocks. *Biology Letters*, **12**(4): 20150975.

Panyutina AA, Kuznetsov AN, Volodin IA, et al. 2017. A blind climber: THE first evidence of ultrasonic echolocation in arboreal mammals. *Integrative Zoology*, **12**(2): 172–184.

Piao ZJ. 2019. The docile *Sicista caudata*. *Forest & Humankind*, (5): 94–99. (in Chinese).

Pisano J, Condamine FL, Lebedev V, et al. 2015. Out of Himalaya: the impact of past Asian environmental changes on the evolutionary and biogeographical history of Dipodoidea (Rodentia). *Journal of Biogeography*, **42**(5): 856–870.

Pyron RA. 2015. Post-molecular systematics and the future of phylogenetics. *Trends in Ecology & Evolution*, **30**(7): 384–389.

Qiu ZD, Li Q. 2016. Neogene Rodents from Central Nei Mongol, China. Beijing: Science Press, 173–206. (in Chinese).

Qiu ZD, Storch G. 2000. The early Pliocene micromammalian fauna of bilike, Inner Mongolia, China (Mammalia: Lipotyphla, Chiroptera, Rodentia, Lagomorpha). *Senckenbergiana Lethaea*, **80**(1): 173–229.

Rambaut A, Drummond AJ, Xie D, et al. 2018. Posterior summarization in Bayesian phylogenetics using tracer 1.7. *Systematic Biology*, **67**(5): 901–904.

Reichgelt T, Baumgartner A, Feng R, et al. 2023. Poleward amplification, seasonal rainfall and forest heterogeneity in the Miocene of the eastern USA. *Global and Planetary Change*, **222**: 104073.

Ronquist F, Teslenko M, van der Mark P, et al. 2012. MrBayes 3.2: efficient Bayesian phylogenetic inference and model choice across a large model space. *Systematic Biology*, **61**(3): 539–542.

Rusin M, Lebedev V, Matrosova V, et al. 2018. Hidden diversity in the Caucasian mountains: an example of birch mice (Rodentia, Sminthidae, *Sicista*). *Hystrix, the Italian Journal of Mammalogy*, **29**(1): 61–66.

Savinov PF. 1970. Jerboas (Dipodidae, Rodentia) from the Neogene of Kazakhstan. *In*: Flerov KK. Material on Evolution of Terrestrial Vertebrates. Moscow: Nauka, 91–134. (in Russian).

Shenbrot G, Bannikova A, Giraudoux P, et al. 2017. A new recent genus and species of three-toed jerboas (Rodentia: Dipodinae) from China: a living fossil?. *Journal of Zoological Systematics and Evolutionary Research*, **55**(4): 356–368.

Shenbrot G, Sokolov V, Heptner V. 2008. Mammals of Russia and Adjacent Regions: Jerboas. New Delhi: Amerind Publishing, 6–173.

Sinitsa MV, Tleuberdina PA, Pita OM. 2024. Squirrels (Rodentia, Sciuridae) from the Late Miocene Pavlodar fossil site in northern Kazakhstan: implications for cranial anatomy and evolutionary history of the early marmotine ground squirrel genus *Sinotamias*. *Historical Biology*, **36**(12): 2804–2816.

Song ZH, Wan SM, Colin C, et al. 2021. Paleoenvironmental evolution of South Asia and its link to Himalayan uplift and climatic change since the late Eocene. *Global and Planetary Change*, **200**: 103459.

Stadler T. 2010. Sampling-through-time in birth-death trees. *Journal of Theoretical Biology*, **267**(3): 396–404.

Suchard MA, Lemey P, Baele G, et al. 2018. Bayesian phylogenetic and phylodynamic data integration using BEAST 1.10. *Virus Evolution*, **4**(1): vey016.

Sun JM, Zhu RX, Bowler J. 2004. Timing of the Tianshan Mountains uplift constrained by magnetostratigraphic analysis of molasse deposits. *Earth and Planetary Science Letters*, **219**(3-4): 239–253.

Swofford DL. 2002. PAUP*: Phylogenetic analysis using parsimony (*and other methods), Version 4.0b10. Sunderland: Sinauer Associates.

Tesakov AS, Titov VV, Simakova AN, et al. 2017. Late Miocene (Early Turolian) vertebrate faunas and associated biotic record of the Northern Caucasus: geology, palaeoenvironment, biochronology. *Fossil Imprint*, **73**(3-4): 383–444.

Wang XM, Qiu ZD, Li Q, et al. 2009. A new early to late Miocene fossiliferous region in central Nei Mongol: lithostratigraphy and biostratigraphy in Aoerban strata. *Vertebrata Palasiatica*, **47**(2): 111–134.

Wickham, H. 2016. Ggplot2: Elegant Graphics for Data Analysis. 2nd ed. Cham: Springer International Publishing.

Wu SY, Zhang FC, Edwards SV, et al. 2014. The evolution of bipedalism in jerboas (Rodentia: Dipodoidea): origin in humid and forested environments. *Evolution*, **68**(7): 2108–2118.

Wysocki CJ, Katz Y, Bernhard R. 1983. Male vomeronasal organ mediates female-induced testosterone surges in mice. *Biology of Reproduction*, **28**(4): 917–922.

Wysocki CJ, Lepri JJ. 1991. Consequences of removing the vomeronasal

organ. *The Journal of Steroid Biochemistry and Molecular Biology*, **39**(4B): 661–669.

Xie JM, Chen YR, Cai GJ, et al. 2023. Tree Visualization By One Table (tvBOT): a web application for visualizing, modifying and annotating phylogenetic trees. *Nucleic Acids Research*, **51**(W1): W587–W592.

Xiong ZY, Liu XH, Ding L, et al. 2022. The rise and demise of the Paleogene Central Tibetan Valley. *Science Advances*, **8**(6): eabj0944.

Yu Y, Blair C, He XJ. 2020. RASP 4: ancestral state reconstruction tool for multiple genes and characters. *Molecular Biology and Evolution*, **37**(2): 604–606.

Zachos J, Pagani M, Sloan L, et al. 2001. Trends, rhythms, and aberrations in global climate 65 Ma to present. *Science*, **292**(5517): 686–693.

Zagorodniuk I. 2021. The incisive foramen as character in distinguishing morphologically similar species of mammals. *Theriologia Ukrainica*, **22**: 63–68.

Zhang D, Gao FL, Jakovlić I, et al. 2020. PhyloSuite: an integrated and scalable desktop platform for streamlined molecular sequence data management and evolutionary phylogenetics studies. *Molecular Ecology Resources*, **20**(1): 348–355.

Zhang Q, Xia L, Kimura Y, et al. 2013. Tracing the origin and diversification of Dipodoidea (Order: Rodentia): evidence from fossil record and molecular phylogeny. *Evolutionary Biology*, **40**(1): 32–44.

Zhao L, Lu HY, Tang LY. 2018. Cenozoic palynological records and vegetation evolution in the Weihe Basin, Central China. *Quaternary Sciences*, **38**(5): 1083–1093. (in Chinese).

Zhu WL, Ding L, Ji YF, et al. 2022. Subduction evolution controlled Himalayan orogenesis: implications from 3-D subduction modeling. *Applied Sciences*, **12**(15): 7413.